

CHAPTER II

THEORY

2.1 Introduction to Zeolites

Among the industrial used catalysts, zeolites are one of the most useful catalysts. Zeolites are crystalline aluminosilicates of alkaline and alkaline-earth metals. They possess many desirable ion-exchange, molecular sieving, and catalytic properties, which make them valuable mineral commodities [5]. Synthetic zeolites have been used for over 25 years in commercial processes, but only recently have mineral zeolites been as potentially valuable mineral commodities [1].

Zeolites were first identified by Constedt in 1756 [6]. The name zeolite, from the Greek words meaning "boiling stone", alludes to the frothing and bubbling observed by Constedt when he heated several crystals. In 1845, Way discovered that certain soils retained ammonium salts. Breck [5] reported that hydrated silicated in the soil were found to be responsible and that these were probably the first ion-exchange experiments. Weigel and Steinhoff, in 1925, were the first to determine that chabazite selectively absorbed smaller organic molecules and rejected large molecules. This phenomenon was described by McBain [7] in 1932 as "molecular sieving".

As knowledge of the properties of zeolites increased, it became apparent that they could be utilized for industrial processes. Zeolites, however, were considered to be mineralogical curiosities that filled vugs and fractures in igneous rocks. The synthesis of zeolite was reported as early as 1862, although Breck [8] noted that the early work was not substantiated by X-ray diffraction and some of it is not

reproducible. He credited Barrer with the first synthesis of analcime-type zeolites substantiated by X-ray diffraction in 1951.

Initially, zeolites were synthesized under temperatures and pressures thought to be responsible for the crystallization of zeolites in basaltic rocks [8]. Breck reports that in 1959, Milton and coworkers at Union Carbide Corp. developed a new technique that allowed low-temperature synthesis of zeolites. Their technique used extremely reactive components in a closed system and temperature of crystallization more typical of those for organic compounds. This procedure was adaptable to large-scale production of synthetic zeolites [8].

By 1980's, 40 natural zeolites had been identified (table 2.1), over 100 zeolites had been synthesized. Approximately 163,000 st of natural and synthetic zeolites were consumed in the United States in 1980. While synthetic zeolites have been used extensively in commercial applications, demand for natural zeolites has been limited. Their primary use is in areas where the use of synthetic zeolites would be uneconomical. Several uses, both commercial and experimental, include ammonium-ion removal for aquaculture and uranium mine waste water, odor control for chicken farming and cat litter, and removal of heavy metal ions from nuclear, mine, and industrial waste waters.

For the definitions of zeolites, zeolites are crystalline-framework aluminosilicates based on a three-dimensional network of SiO_4 tetrahedra, with all four oxygens shared by adjacent tetrahedra. Zeolites may be represented by the empirical formula $\text{M}_{2/n} \cdot \text{Al}_2\text{O}_3 \cdot x\text{SiO}_2 \cdot y\text{H}_2\text{O}$. M is an alkali or alkaline earth cation of valence, x is a number between 2 and 10, and y is a number between 2 and 7. The principle cations are sodium, potassium, magnesium, calcium, strontium, and barium. The cations are loosely bound in the structure

Table 2.1 Dates of discovery of 40 zeolites

Stilbite	1756	Clinoptilolite	1890
Natrolite	1758	Offretite	1890
Chabazite	1772	Erionite	1890
Harmotome	1775	Kehoeite	1893
Analcime	1784	Gonnardite	1896
Laumontite	1785	Dachiardite	1905
Thomsonite	1801	Stellerite	1909
Scolecite	1801	Ferrierite	1918
Heulandite	1801	Viseite	1942
Gmelinite	1807	Yugawaralite	1952
Mesolite	1813	Wairakite	1955
Gismondine	1816	Bikitaite	1957
Brewsterite	1822	Paulingite	1960
Epistilbite	1823	Garronite	1962
Phillipsite	1824	Mazzite	1972
Levynite	1825	Barrerite	1974
Herschelite	1825	Cowlesite	1975
Edingtonite	1825	Merlinoite	1976
Faujasite	1842	Svetlozarite	1976
Mordenite	1864	Amicite	1979

ศูนย์วิทยทรัพยากร
จุฬาลงกรณ์มหาวิทยาลัย

and may be exchanged, to varying degrees, by each other. The framework contains channels and interconnected voids occupied by cations and water molecules. Most zeolites can be reversibly dehydrated.

Zeolites are characterized by the following properties [8]:

1. High degree of hydration.
2. Low density and large void volume when dehydrated.
3. Stability of the crystal structure of many zeolites when dehydrated.
4. Cation exchange properties.
5. Uniform molecular-sized channels in dehydrated crystals.
6. Various physical properties such as electrical conductivity.
7. Adsorption of gases and vapors.
8. Catalytic properties.

Molecular sieves are materials that, because of their internal structure, can selectively adsorb molecules according to their size and/or shape. All zeolites are molecular sieves, but not all molecular sieves are zeolites. Activated carbon, activated clay, alumina powder, and silica gels are examples of molecular sieves that are not zeolites [8].

2.2 Classifications of Zeolite Structures

Zeolites are crystalline frameworks of oxygen, aluminum, and silicon extending in a three-dimensional framework. The first classification of zeolites on the basis of common structural units such as parallel 6-rings was made by Smith [9]. Meier classified zeolites into seven groups within each group, zeolites have a common subunit of structure which is a specific array of $(Al, Si)O_4$ tetrahedra. These tetrahedra are then grouped together to form secondary building unit (SBU's). There are eight SBU's: the single 4-ring (S4R), the single 6-ring (S6R), the single 8-ring (S8R), the double 4-ring (D4R), the double

6-ring(D6R), the natrolite unit(4-1), the mordenite unit(5-1), and the stilbite unit(4-4-1)(fig.2.1). These units are sufficient to describe a zeolite framework although 3 and 9 rings should be added. This classification into seven groups should be extended to nine groups with the addition of melanopholite group based on the aluminosilicate analogs of the gas hydrates and the lovdarite group based on 3,5 and 9 rings.

The nine groups of zeolites identified on the basis of their framework structure are given in table 2.2 with idealized cell contents and crystallographic data and channel systems.

Analcite Group

The frameworks of the two members of this group, analcite and laumontite, can be derived by interconnecting 4 and 6-rings as shown in fig.2.2.

Natrolite Group

The chains (fig.2.3a) characteristic of this group consist of linked four 4-ring units. These are three different ways to link these chains resulting in the natrolite, edingtonite, and thomsonite frameworks(fig.2.4). All the structures have a two dimensional 8-ring channel system.

Chabazite Group

The chabazite group frameworks consists of parallel 6-rings. The offretite-erionite a and c projections are shown in figs. 2.4a - 2.4d. The stacking sequence involves single 6-rings A, B or C. double 6-rings AA, BB or CC or a combination of both. The stacking sequence of the members of the group are:

Cancrinite	AB	Levynite	AABCCABBC
Gmelinite	AABB	Afghanite	ABABACAC
Chabazite	AABBC	Losod	ABAC

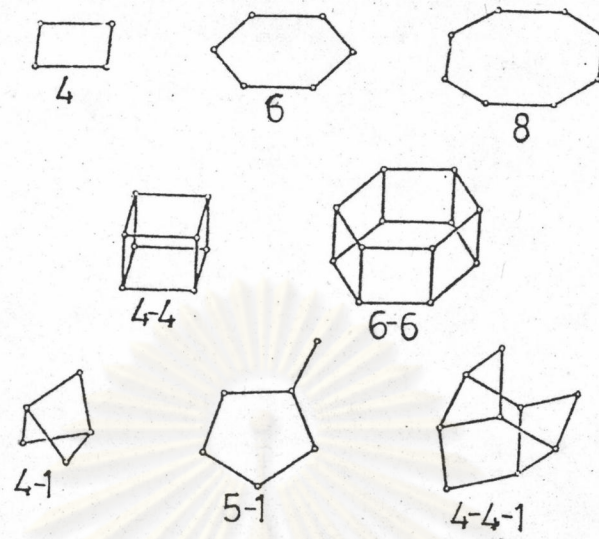


Figure 2.1 Secondary Building Units

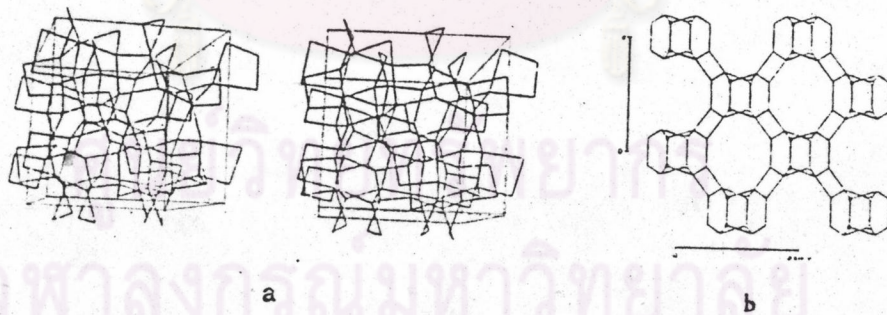


Figure 2.2 Framework of (a) analcite (b) laumontite

Table 2.2 Classification and crystallographic data for zeolites

	Typical Unit Cell Contents	Crystal Data	Framework Density	Channel System
Analcite Group				
Analcite	$\text{Na}_{16}(\text{AlO}_2)_{16}(\text{SiO}_2)_{32} \cdot 16\text{H}_2\text{O}$	Cubic Ia3d a=13.7Å	18.6 ^d	
Laumontite	$\text{Ca}_4(\text{AlO}_2)_8(\text{SiO}_2)_{16} \cdot 16\text{H}_2\text{O}$	Monoclinic Am or A2 a=7.6, b=14.8, c=13.1Å, $\gamma=112^\circ$	17.7	10 ^b (4.0x5.6) ^{c,d}
Natrolite Group				
Natrolite	$\text{Na}_{16}(\text{AlO}_2)_{16}(\text{SiO}_2)_{24} \cdot 16\text{H}_2\text{O}$	Orthorhombic Fdd2 a=18.3, b=18.6, c=13.2Å	17.8	8(2.6x3.9)3
Thomsonite	$\text{Na}_4\text{Ca}_8(\text{AlO}_2)_{20}(\text{SiO}_2)_{20} \cdot 24\text{H}_2\text{O}$	Orthorhombic Pnn2 a=13.1, b=13.1, c=13.2Å	17.7	8(2.6x3.9)3
Edingtonite	$\text{Ba}_2(\text{AlO}_2)_4(\text{SiO}_2)_6 \cdot 8\text{H}_2\text{O}$	Orthorhombic P2 ₁ 2 ₁ 2 ₁ a=9.6, b=9.7, c=6.5Å	16.6	8(3.5x3.9)3
Chabazite Group				
Chabazite	$\text{Ca}_2(\text{AlO}_2)_4(\text{SiO}_2)_8 \cdot 13\text{H}_2\text{O}$	Trigonal R3m a=13.2, c=15.1	14.6	8(3.6x3.7)3
Gmelinite	$\text{Na}_8(\text{AlO}_2)_8(\text{SiO}_2)_{16} \cdot 24\text{H}_2\text{O}$	Hexagonal P6 ₃ /mmc a=13.8, c=10.0Å	14.6	12(7.0)1 ^e 8(3.6x3.9)2
Erionite	$(\text{Ca}, \text{MgNa}_2\text{K}_2)_4 \cdot 5(\text{AlO}_2)_9(\text{SiO}_2)_{27} \cdot 27\text{H}_2\text{O}$	Hexagonal P6 ₃ /mmc a=13.3, c=15.1Å	15.6	8(3.6x5.2)3
Offretite	$(\text{K}_2, \text{Ca}, \text{Mg})_{2.5}(\text{AlO}_2)_5(\text{SiO}_2)_{13} \cdot 15\text{H}_2\text{O}$	Hexagonal P6m2 a=13.3, c=7.6Å	15.5	12(6.4)1 ^e 8(3.6x5.2)2
Levynite	$\text{Ca}_3(\text{AlO}_2)_6(\text{SiO}_2)_{12} \cdot 18\text{H}_2\text{O}$	Trigonal R3m a=13.3, c=23.0Å	15.2	8(3.3x5.3)2
Mazzite	$\text{Na}_6\text{K}_{1.9}\text{Ca}_{1.4}\text{Mg}_2(\text{AlO}_2)_9 \cdot 8(\text{SiO}_2)_{26.5} \cdot 28\text{H}_2\text{O}$	Hexagonal P6 ₃ /mmc a=18.4, c=7.6Å	16.1	12(7.4)1
Linde L	$\text{K}_6\text{Na}_3(\text{AlO}_2)_9(\text{SiO}_2)_{27} \cdot 8\text{H}_2\text{O}$	Hexagonal P6/mmm a=18.4, c=7.5Å	16.4	12(7.1)1
Afghanite	$(\text{Na}_2\text{CaK})_{12}(\text{AlO}_2)_{24}(\text{SiO}_2)_{24} - (\text{Na}_2\text{CaK})_6(\text{Cl}_2, \text{SO}_4, \text{CO}_3)_6$	Hexagonal P6 ₃ /mmc a=12.8, c=10.5Å	15.9	6
Losod	$\text{Na}_{12}(\text{AlO}_2)_{12}(\text{SiO}_2)_{12} \cdot 19\text{H}_2\text{O}$	Hexagonal P62c a=12.9, c=10.5Å	15.8	6
Liottite	$(\text{CaNa}_2\text{K}_2)_9(\text{AlO}_2)_{18}(\text{SiO}_2)_{18} - (\text{CaNa}_2\text{K}_2)_n(\text{SO}_4, \text{CO}_3, \text{Cl})_8 \cdot 2\text{H}_2\text{O}$	Hexagonal P6m2 a=12.8, c=5.1Å	15.7	6
TMA-E (AB)	$(\text{Me}_4\text{N})_2\text{Na}_7(\text{AlO}_2)_9(\text{SiO}_2)_{27} \cdot 26\text{H}_2\text{O}$	Hexagonal P6 ₃ /mmc a=13.3, c=15.2Å	15.4	8(3.7x4.8)2
Cancrinite	$\text{Na}_6(\text{AlO}_2)_6(\text{SiO}_2)_6 \cdot \text{CaCO}_3 \cdot 2\text{H}_2\text{O}$	Hexagonal P6 ₃ a=12.8, c=5.1Å	16.7	12(6.2)1

Table 2.2 Classification and crystallographic data for zeolites
(continued)

Phillipsite Group	Typical Unit Cell Contents	Crystal Data	Framework Density	Channel System
Phillipsite	$(KNa)_5(AlO_2)_5(SiO_2)_{11} \cdot 10H_2O$	Monoclinic P2 ₁ /m a=9.9, b=14.3, c=8.7A β=124°	15.8	8(4.2x4.4)1 ^e 8(2.8x4.8) 8(3)1
Gismondite	$Ca_4(AlO_2)_8(SiO_2)_8 \cdot 16H_2O$	Monoclinic P2 ₁ /a a=9.8, b=10.0 c=10.6A, γ=90°	15.4	8(3.1x4.4)1 ^e 8(2.8x4.9)1
Yugawaralite	$Ca_4(AlO_2)_8(SiO_2)_{20} \cdot 16H_2O$	Monoclinic Pc a=6.7, b=14.0, c=10.0A, β=112°	18.3	8(3.1x3.5)1 ^e 8(3.2x3.3)1
Li A (BW)	$Li_4(AlO_2)_4(SiO_2)_4 \cdot 4H_2O$	Orthorhombic Pna2 a=10.3, b=8.2, c=5.0A	19.0	8(3.6x4.0)1
<u>Heulandite Group</u>				
Heulandite	$Ca_4(AlO_2)_8(SiO_2)_{28} \cdot 24H_2O$	Monoclinic Cm a=17.7, b=17.9, c=7.4A, β=116°	17.0	8(4.0x5.5)1 ^e 10(4.4x7.2)1 8(4.1x4.7)1
Brewsterite	$(Sr,Ba,Ca)_2(AlO_2)_4(SiO_2)_{12} \cdot 10H_2O$	Monoclinic P2 ₁ /m a=6.8, b=17.5, c=7.7A, β=95°	17.5	8(2.3x5.0)1 ^e 8(2.7x4.1)1
Stilbite	$Na_2Ca_4(AlO_2)_{10}(SiO_2)_{26} \cdot 32H_2O$	Monoclinic F 2/m a=13.6, b=18.2, c=17.8A, β=91°	16.9	10(4.1x6.2)1 ^e 8(2.7x5.7)1
<u>Mordenite Group</u>				
Mordenite	$Na_8(AlO_2)_8(SiO_2)_{40} \cdot 24H_2O$	Orthorhombic Cmcm a=18.1, b=20.5, c=7.5A	17.2	12(6.7x7.0)1 ^e 8(2.9x5.7)1
Ferrierite	$Na_{1.5}Mg_2(AlO_2)_{5.5}(SiO_2)_{30.5} \cdot 18H_2O$	Orthorhombic Immm a=19.2, b=14.1, c=7.5A	17.7	10(4.3x5.5)1 ^e 8(3.4x4.8)1
Dachiardite	$Na_5(AlO_2)_5(SiO_2)_{19} \cdot 12H_2O$	Monoclinic C2/m a=18.7, b=7.5, c=10.3A, β=108°	17.3	10(3.7x6.7)1 ^e 8(3.6x4.8)1 ^e
Bikitaite	$Li_2(AlO_2)_2(SiO_2)_4 \cdot 2H_2O$	Monoclinic P2 ₁ a=7.6, b=8.6, c=5.0A, γ=114°	20.2	8(3.2x4.9)1
Epistilbite	$Ca_3(AlO_2)_6(SiO_2)_{18} \cdot 16H_2O$	Monoclinic C2/m a=8.9, b=17.7, c=10.2, β=124°	18.0	10(3.5x5.3)1 ^e 8(3.7x4.4)1
ZSM-5	$Na_n(AlO_2)_n(SiO_2)_{96-n} \cdot 16H_2O$ n<27	Orthorhombic Pnma a=20.1, b=19.9, c=13.4A	17.9	10(5.4x5.6)1 ^e 10(5.1x5.5)1 ^e
ZSM-11	$Na_n(AlO_2)_n(SiO_2)_{96-n} \cdot 16H_2O$ n<27	Tetragonal I4m2 a=20.1, c=13.4A	17.7	10(5.1x5.5)1 ^e

Table 2.2 Classification and crystallographic data for zeolites
(continued)

Faujasite Group	Typical Unit Cell Contents	Crystal Data	Framework Density	Channel System
Faujasite	$\text{Na}_{12}\text{Ca}_{12}\text{Mg}_{11}(\text{AlO}_2)_{59}(\text{SiO}_2)_{133} \cdot 260\text{H}_2\text{O}$	Cubic Fd3m a=24.7Å	12.7	12(7.4)3
Linde A	$\text{Na}_{12}(\text{AlO}_2)_{12}(\text{SiO}_2)_{12} \cdot 27\text{H}_2\text{O}$	Cubic Fm3c (Fm3m) a=24.6Å (a=12.3Å)	12.9	8(4.1)3
ZK-5	$\text{Na}_{30}(\text{AlO}_2)_{30}(\text{SiO}_2)_{66} \cdot 98\text{H}_2\text{O}$	Cubic Im3m a=18.7Å	14.7	8(3.9)3 ^b 8(3.9)3
ZSM-3	$(\text{LiNa})_2(\text{AlO}_2)_2(\text{SiO}_2)_{3.2} \cdot 8\text{H}_2\text{O}$ ^m	Hexagonal a=17.5, c=129Å		
zeolite Rho	$(\text{Na,Cs})_{12}(\text{AlO}_2)_{12}(\text{SiO}_2)_{36} \cdot \text{H}_2\text{O}$	Cubic I43m a=15.1Å	14.3	8(3.9x5.1)3
Paulingite	$(\text{K}_2, \text{Na}_2, \text{Ca}, \text{Ba})_{76}(\text{AlO}_2)_{152}(\text{SiO}_2)_{525} \cdot 700\text{H}_2\text{O}$	Cubic Im3m a=35.1Å	15.5	8(3.9)3 ^d 8(3.9)3
Merlinoite	$(\text{K}_5, \text{Ca}_2)(\text{AlO}_2)_9(\text{SiO}_2)_{23} \cdot 24\text{H}_2\text{O}$	Orthorhombic Immm a=14.1, b=14.2, c=10.0Å	16.0	8(3.1x3.5)1 ^e 8(3.5x3.5)1 8(3.4x5.1)1
Linde N	$\text{Na}_{384}(\text{AlO}_2)_{384}(\text{SiO}_2)_{384} \cdot 518\text{H}_2\text{O}$	Cubic Fd3 a=36.93		6-rings 6-rings
Sodalite	$\text{Na}_6(\text{AlO}_2)_6(\text{SiO}_2)_6 \cdot 2\text{NaCl}$	Cubic P43n a=8.9Å		
Melanophlogite Group				
Melanophlogite	$\text{Me}_n(\text{AlO}_2)_n(\text{SiO}_2)_{48-n} \cdot n\text{H}_2\text{O}$	Cubic P4232 a=13.4Å		6-rings
ZSM-39	$(\text{Na}, \text{TMA}, \text{TEA})_{0.4}(\text{AlO}_2)_{0.4}(\text{SiO}_2)_{135.6} \cdot m\text{H}_2\text{O}$	Cubic Fd3m a=19.4Å	18.7	6-rings
Lovdarite Group				
Lovdarite	$\text{K}_4\text{Na}_{12}(\text{BeO}_2)_8(\text{SiO}_2)_{28} \cdot 18\text{H}_2\text{O}$	Tetragonal Poly type P4 ₂ /mnc a=7.14, b=7.14, c=21.0Å Poly type I4 ₂ m2 a=7.15, b=7.15, c=42		8-ring 1 ^e 9-ring 2 8-ring 9-ring 2

a. Number of atoms per 100Å³.

b. Number of ring members in channel opening.

c. Ring dimension.

d. Dimensions of channel system.

e. Channel system intersect.

f. Separate channel systems.

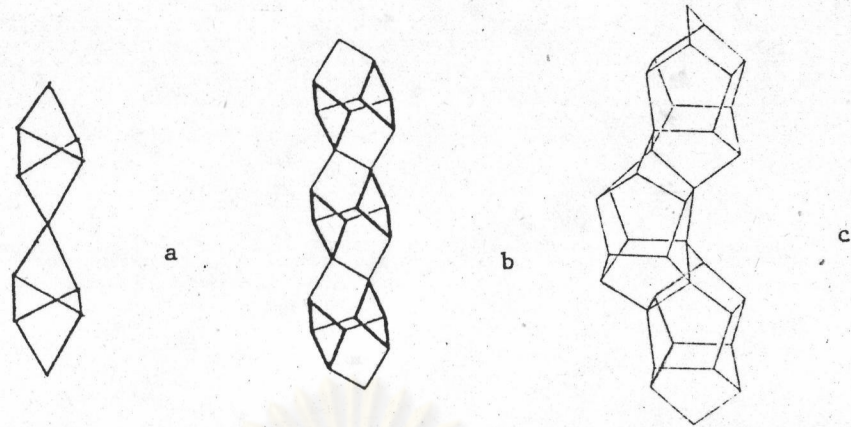


Figure 2.3 Chains in (a) natrolite (b) Brewsterite
(c) ZSM-5

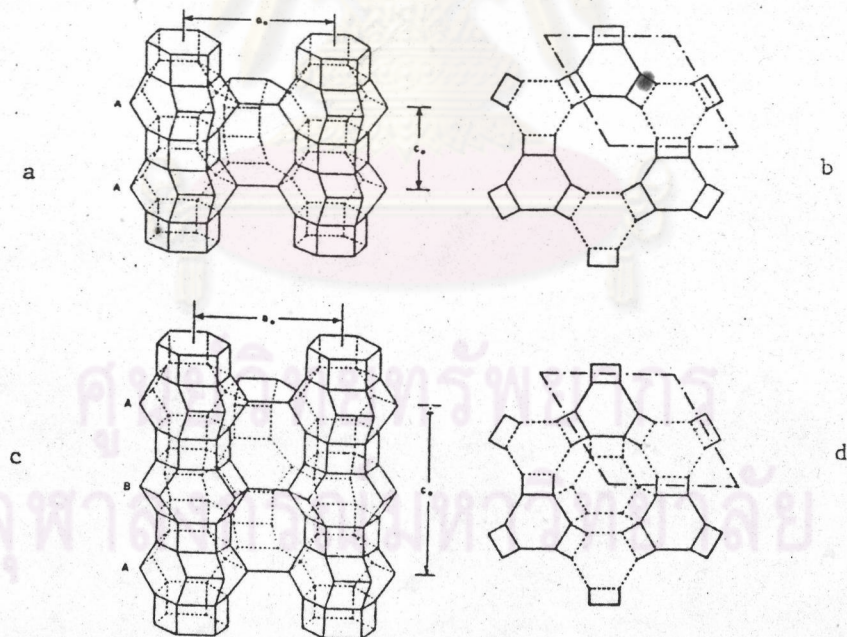


Figure 2.4 Offretite and Erionite Framework (a) offretite
(b) c- projection of offretite (c) erionite (d) c-projection of
erionite

Offretite	AAB	Liottite	ABABAC
Erionite	AABAAC	TMA-E(AB)	ABBACC

The framework of mazzite consists of columns of gmelinite cages linked through 8-rings with alternate columns staggered by $c/2$ (fig. 2.5). If cancrinite cages are connected through double 6-rings to form columns and these columns are linked through 6-rings to form 12-ring channels parallel to the C-axis, as in mazzite, the framework of Linde L is formed.

Phillipsite Group

The framework of members of this group are based on 4-rings with variations of U (up) and D (down) linkages. Three of the four such variations can be linked to form chains (fig. 2.6). Phillipsite and gismondite consist of cross-linked UUDD chains. Li-A (BW) and yugawaralite consist of linked single 4-rings.

Heulandite Group

A building block containing four 5-rings and two 4-rings is common to the framework of all the members of this group. If linked through a common edge, chains are formed (fig. 2.3b) which when linked together yield brewsterite. Linking these blocks through common vertices yield chains which are constituents of heulandite and stibite. This group of structures contain some 5-rings.

Mordenite Group

The secondary building block consisting of four 5-rings is common to all members of this group except bikitaite. In mordenite and dachiardite they are linked to form complex chains which in turn are linked in different ways. Epistilbite and ferrierite are lamellar structures and they also contain the building block in fig. 2.7b. The lamellae are normal to a in ferrierite and to b in epistilbite. The projections along the main channels are shown in figs. 2.8a-e [10]. The

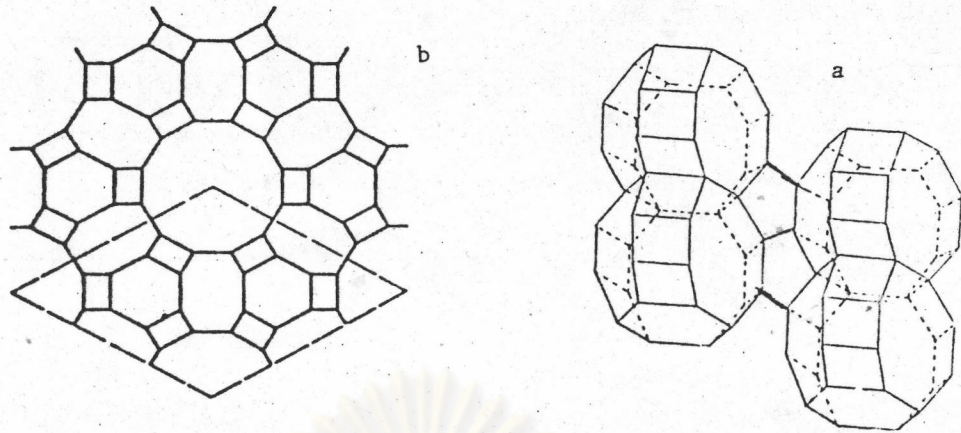


Figure 2.5 Framework of mazzite (a) c-projection (b) linking of gmelinite columns

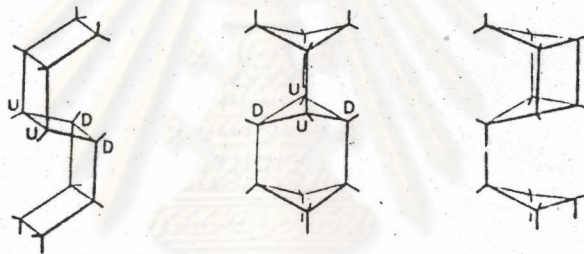


Figure 2.6 Three types of 4-ring chains UDD, UDUD, and UDUU

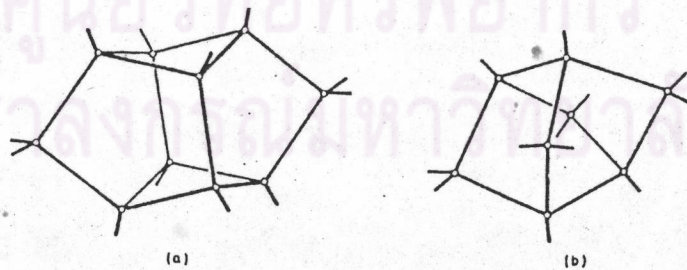


Figure 2.7 Secondary Units in (a) heulandite (b) mordenite group

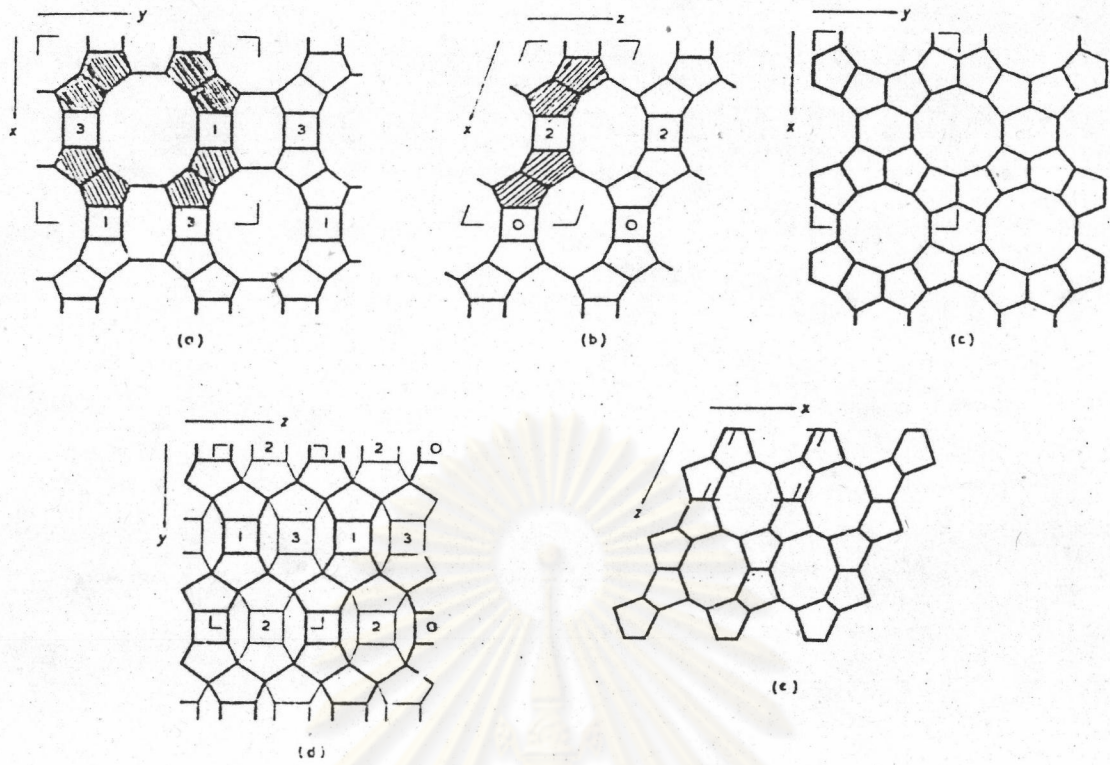


Figure 2.8 Framework projections along main channels of (a) mordenite (b) dachiardite (c) ferrierite (d) epistilbite (e) bikitaite

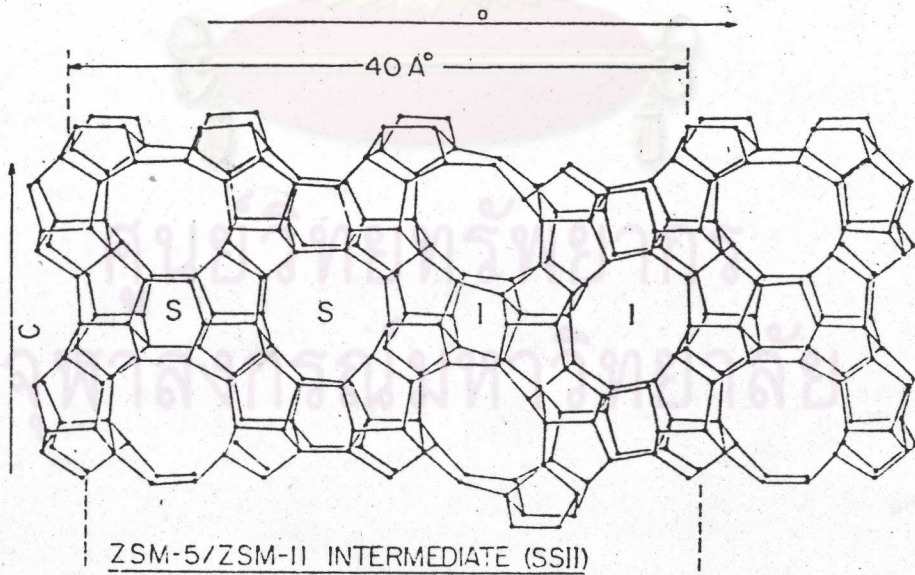


Figure 2.9 Pentasil framework with SSII sequence

projection of bikitaite along b is essentially the same as the projection of epistilbite along a and dachiardite along c . ZSM-5 and ZSM-11 are better described by the chain in fig. 2.3c. The configurational unit in this chain contains eight 5-rings. If these chains are linked so that alternate pairs are related by a reflection, a layer is formed which is the basic layer in the ZSM-5 and ZSM-11 structures. If this layer is linked so that alternate layers are related by a reflection, S , the ZSM-11 framework is formed. If the layers are linked such that alternate layers are related by an inversion I , the ZSM-5 framework results. If the stacking sequence is varied, a family of structures results with ZSM-5 and ZSM-11 as the end members. With the lattice parameter doubled there are only two possible stacking sequences, SSII and SISI. The framework for SSII is shown in fig. 2.9. This variation in stacking sequence has been confirmed by Thomas and Millward [11] with lattice imaging using ultra high resolution electron microscopy.

Faujasite Group

There are three types of cages in this group, sodalite, A and ZK-5. Linde A is formed by linking sodalite cages through double 4-rings. The large cages in Linde A will be referred to as the A cage. If the A cages are linked through double 6-rings, the framework of ZK-5 is formed. If they are linked through double 8-rings, the rho structure results (fig. 2.10). The cage formed by the octagonal faces of the A cages in ZK-5 is analogous to the gmelinite cage and will be referred to as the ZK-5 cage. Columns of ZK-5 cages linked through double 8-rings when connected together form the merlinoite framework. Feldspar and phillipsite are closely related to merlinoite formed by sliding layers such that the double 8-rings are broken up. Figure 10a shows part of the framework of paulingite, the sequence of cages along

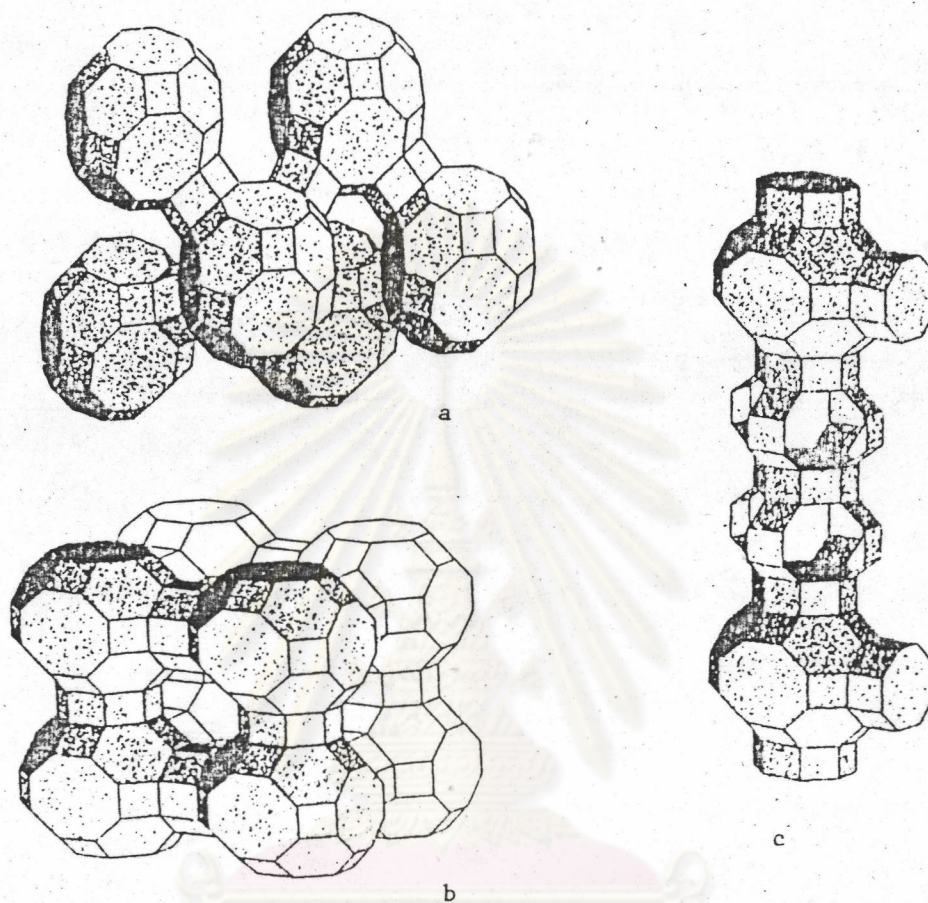


Figure 2.10 Arrangement of a cages in (a) ZK-5 (b) Paulingite

the cubic axis A, ZK-5, ZK-5, A each connected to the other through double 8-rings. No one cage can be considered as the building block, the combination of cages is required.

The faujasite framework consists of sodalite cages linked through double 6-rings. If layers of these connected sodalite cages are linked in an ABC sequence the framework is that of faujasite with Fd3m symmetry, the same as diamond.

If the stacking sequence is changed to AB, the result is a hexagonal structure. There are now five 12-ring openings to the large cavity compared to four in faujasite. The c parameter and the number of stacking sequences is dependent on the number of layers in the identity period. ZSM-3 [12] was found to be hexagonal with $a=17.5$ and $c=129 \text{ \AA}$ indicating a nine layer stacking sequence.

Sodalite cages linked through common 6-rings form the sodalite framework .

Falsh and Anderson found that Linde N, a cubic structure with $a=36.9\text{\AA}$, was an intergrowth of ZK-5 and sodalite.

Melanophlogite Group

The relationship between hydrogen bonds linking oxygens in gas hydrates (clathrates) and oxygens linking T-atoms in zeolites is well known. Hexagonal ice I is isostructural with B-tridymite. Appleman found that the rare mineral melanophlogite is isostructural with the 12A cubic gas hydrate. The melanophlogite framework consists of interwoven layers of 12 and 14-hedra (figs. 2.11 and 2.12). It is a dense structure with only 5 and 6-ring openings. ZSM-39, a high silica synthetic zeolite, was found to be isostructural with the 17A cubic gas hydrate. The ZSM-39 framework consists of 12 and 16-hedra as shown in fig. 2.11, with layers of face sharing 12-hedra arranged as in fig. 2.13. These layers are stacked in ABC sequence. The openings in the

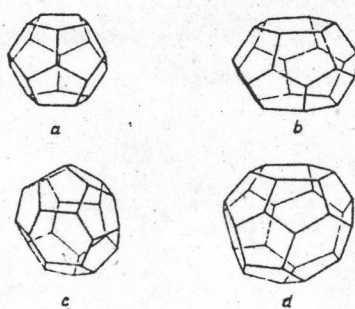


Figure 2.11 Polyhedral units in ZSM-39 and Melanopholgite structure
(a) 12-hedron (b) 14-hedron (c) 15-hedron (d) 16-hedron

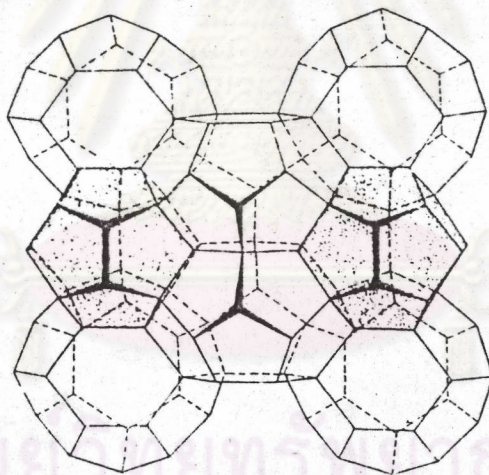


Figure 2.12 Melanopholgite framework

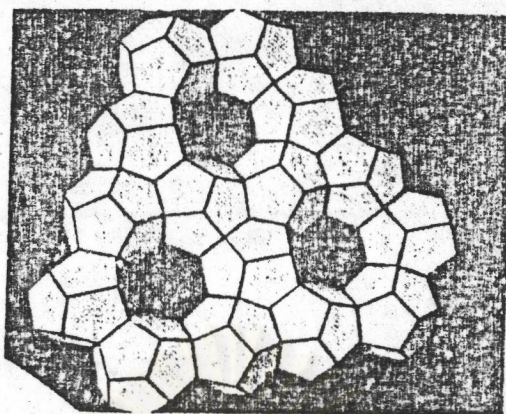


Figure 2.13 ZSM-39 framework

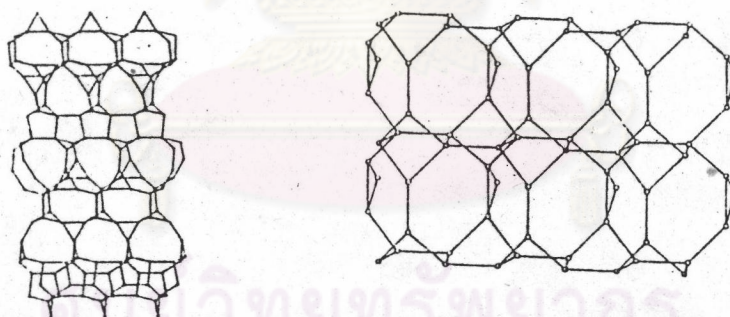


Figure 2.14 Lovdarite framework (a) a-axis projection (b) c-axis projection

framework are limited to 5 and 6-rings. Zeolite analogs of water clathrate structures which typically consist of cages comprising of 5-rings constitute a new family of zeolites.

Lovdarite Group

Lovdarite, a unique beryllium zeolite, has a framework consisting of 4 and 8-rings linked via corner sharing 3-rings. It has a two dimensional intersecting channel system bounded by 9-rings (fig. 2.14). The 9-rings are unique as no other known zeolite has a 9-ring channel system. The 129° equilibrium angle of the Be-O-Si linkage indicates that the three-membered rings are not strained.

For the other classification, attempts have been made to group together zeolites which have structural elements in common. For numerous synthetic zeolites the structures are still unknown, but examples of grouping are given in table 2.3. This table contains instances of framework anions which are variants of a single topology, i.e. isotypes (egs. all members of the analcime group; heulandite and clinoptilolite in the heulandite group; stilbite, stellerite and barrerite, also in the heulandite group; phillipsite and harmotome in the phillipsite group; gismondine and Na-P also in the phillipsite group; and natrolite, scolecite and mesolite in the natrolite group). Variants of a given topology arise as a result of differing chemical compositions. For example analcime has a cubic unit cell of edge 13.72 Å and unit cell content $\text{Na}_{16}[\text{Al}_{16}\text{Si}_{32}\text{O}_{96}] \cdot 16\text{H}_2\text{O}$. The Na^+ and the H_2O occupy different sub-lattices. Exchange of Na^+ by K^+ gives leucite with a tetragonal unit cell having $a = 12.98 \text{ \AA}$ and $c = 13.68 \text{ \AA}$. The crystals are anhydrous and the K^+ ions are in the sub-lattice occupied by H_2O in analcime. The topology of the analcime anion is however unchanged. Another way in which variants of a given topology may arise is through changes in Si/Al ratios in the framework. This changes the cation

Table 2.3 Classification of some zeolites and some porous tectosilicates

1. <u>Analcine Group</u>	Stilbite Stellerite Barrerite
Analcime	
Wairakite	
Leucite (felspathoid)	
Rb-analcime (.")	6. <u>Laumontite Group</u>
Pollucite	Laumontite
Viseite (aluminosilico-phosphate)	Yugawaralite
Kehoeite (aluminumphosphate)	7. <u>Mordenite Group</u>
2. <u>Chabazite Group</u>	Mordenite
Chabazite	Ferrierite
Gmelinite	Dachiardite
Erionite	Epistilbite
Offretite	Bikitaite
Levynite	8. <u>Natrolite Group</u>
Mazzite (zeolite Ω)	Natrolite
Zeolite L	Scolecite
Sodalite hydrate	Mesolite
Cancrinite hydrate	Thomsonite
3. <u>Clathrate Group</u>	Gonnardite
Melanophlogite	Edingtonite
Zeolite ZSM-39, Clathrasil-3C	Metanatrolite
4. <u>Faujasite Group</u>	9. <u>Pentasil Group</u>
Faujasite (zeolites X and Y)	Zeolite ZSM-5, Silicalite 1
Zeolite ZSM-2	Zeolite ZSM-11, Silicalite 11
Zeolite ZSM-3	10. <u>Phillipsite Group</u>
Paulingite	Phillipsite
Zeolite A	Harmotome
Zeolite RHO	Gismondine
Zeolite ZK-5	Zeolite Na-P
5. <u>Heulandite Group</u>	Amicite
Heulandite	Carronite
Clinoptilolite	Merlinoite
Brewsterite	Zeolite Li-ABW

density, which can also be altered by exchanges such as $2\text{Na}^+ \rightleftharpoons \text{Ca}^{2+}$. These two factors operate for the isotypes heulandite $\text{Ca}_4[\text{Al}_8\text{Si}_{28}\text{O}_{72}] \cdot 24\text{H}_2\text{O}$, (monoclinic, $a = 17.72 \text{ \AA}$, $b = 17.90 \text{ \AA}$, $c = 7.43 \text{ \AA}$, $B = 116^\circ 25'$) and clinoptilolite, $\text{Na}_6[\text{Al}_6\text{Si}_{30}\text{O}_{72}] \cdot 24\text{H}_2\text{O}$, (monoclinic, $a = 17.64 \text{ \AA}$, $b = 17.90 \text{ \AA}$, $c = 7.40 \text{ \AA}$, $B = 116^\circ 22'$). When one cation is replaced by another of different size or charge the distributions of the ions between sub-lattices may change as well as the water content under ambient conditions. Such changes can in turn cause minor or significant framework distortions without altering the topology. An example of the variation of water content with exchange cation is shown in fig. 2.15 for phillipsite [13]. For ions of the same charge water contents decrease as ion radius increases. A different curve is obtained for series of divalent ions than for a series of univalent ones.

Guest species other than water can also result in variants of a given topology. Sodalite ($\text{Na}_6[\text{Al}_6\text{Si}_6\text{O}_{24}] \cdot 2\text{NaCl}$; cubic with $a = 8.87 \text{ \AA}$) and nosean ($\text{Na}_6[\text{Al}_6\text{Si}_6\text{O}_{24}] \cdot \text{Na}_2\text{SO}_4$; cubic with $a = 9.0 \text{ \AA}$) both have the sodalite framework, slightly dilated in the case of nosean. In general, tectosilicate frameworks although strong and rigid can undergo small adjustments of crystallographic significance.

The majority of the frameworks in most zeolite groups are not variants of a given topology but possess different topologies, with structural similarities which justify their being grouped together. Such classifications are not without alternatives because on a basis of the possession of structural sub-units in common certain zeolites could equally well appear in more than one group. Thus in sodalite placed in the chabazite group 14-hedral cavities exist which are also found in some members of the faujasite group (faujasite and zeolite A). However sodalite and cancrinite are structurally related and cancrinite is well placed in the chabazite group and so is sodalite. The classification of

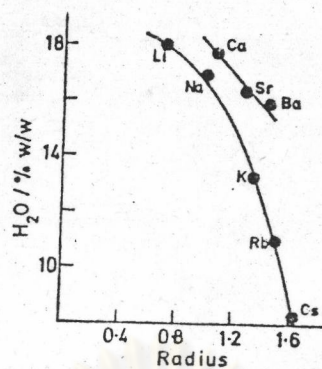


Figure 2.15 Water contents of different cationic forms of phillipsite plotted against cation radii

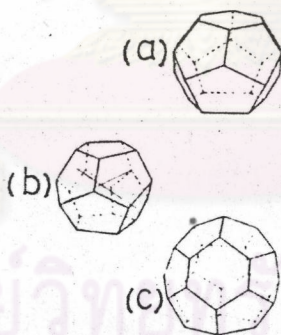


Figure 2.16 Dodecahedra (b), tetradecahedra (a) and hexadecahedra (c) found in melanopholgitite ((a)+(b)) and in dodecasil-3C or zeolite ZSM-39 ((b)+(c))

zeolites into groups is thus somewhat arbitrary.

Zeolites can also be considered in terms of the densities of bonds Si-O-T (T = Al or Si) in the x, y and z directions. Certain network anions have bond densities comparable in all directions (e.g. groups 1, 2, 3, 4 and 9 of table 2.3); others have bond densities greater in two directions than in the third (group 5); and others have these densities greater in one direction than in the remaining two ("fibrous" zeolites of the natrolite group). Bond density differences can influence thermal stability and rigidity and the extent of deformation when undergoing modification by ion exchange or in changes of the Si/Al ratios and in dehydration and rehydration. In the fibrous zeolites the dense-bond chains are cross-linked to like chains by single Si-O-T bonds and this appears to make the frameworks readily deformable. On the other hand in zeolite A 14-hedral sodalite cages are each linked through the six 4-ring faces to six other sodalite cages by four Si-O-T bonds creating a cubic linkage unit. Cross-connecting sodalite cage subunits by multiple Si-O-T bonds produces a more rigid less easily deformable framework than when, as in the natrolite group, crosslinking involves single Si-O-T bonds. Similarly in faujasite each sodalite cage is linked to four other such cages through four of its eight 6-ring faces by six Si-O-T bonds, creating a hexagonal prism linking unit. Rigidity and thermal stability is found for such zeolites as A and faujasite (X and Y) despite the smaller density, greater intracrystalline porosity, and smaller number of (Al + Si) atoms (and hence of Si-O-T bonds) per unit volume. In zeolite A, faujasite, natrolite and thomsonite these numbers are as follows:

Zeolite	natrolite	thomsonite	zeolite A	faujasite
(Al + Si)	14.5	14.4	12.9	12.7
per 1000 Å ³				

Included in table 2.3 are examples of porous crystalline silicas. These are melanophlogite, rare in Nature and only recently synthesised, dodecasil-3C and silicalites I [14] and II. Melanophlogite has the structure of clathrate hydrate type I, in which the pentagonal dodecahedra and tetradecahedra with twelve 5-ring and two 6-ring faces of fig. 2.16 b and a respectively are stacked to fill all space. There are two dodecahedra and six tetradecahedra per cubic unit cell of 13.4 Å edge (fig. 2.17a). In clathrasil-3C as in its isotype ZSM-39 pentagonal dodecahedra are stacked with hexadecahedra having twelve 5-ring and four 6-ring faces to fill all space (fig. 2.17b). There are 6 dodecahedra and 8 hexadecahedra per cubic unit cell of edge 19.4 Å. If there was one guest molecule, G, per void the limiting composition of melanophlogite would be $23\text{SiO}_2 \cdot 2\text{G}$ and that of clathrasil-3C would be $13\text{SiO}_2 \cdot 2\text{G}$. If only the larger voids contained a guest molecule the limiting compositions would be $23\text{SiO}_2 \cdot 3\text{G}$ and $17\text{SiO}_2 \cdot \text{G}$ respectively. Because of their analogy with clathrate hydrates they have been termed the clathrate group in table 2.3. Since a range of clathrate hydrates is known synthesis may reveal more porous silicas or zeolites in this group structurally like their clathrate hydrate counterparts. All are rich in 5-rings and indeed the clathrate, mordenite, heulandite and pentasil zeolite groups are all related in this respect.

The pentasil zeolites ZSM-5 and ZSM-11 and their respective end members silicalites I and II differ from melanophlogite and clathrasil-3C in having relatively open continuous channels rather than semi-isolated voids permeating their structures. A view of their frameworks is shown in fig. 2.18a and b, and a formal representation of the three-dimensional channel patterns in fig. 2.19c and a together with this pattern for an intermediate structure, of which many are possible (fig.

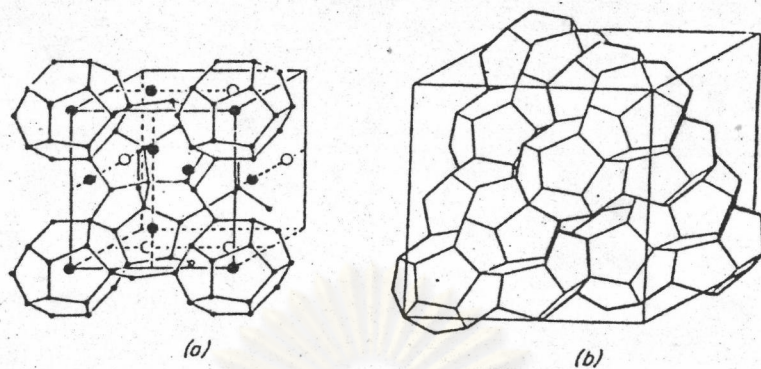


Figure 2.17 Stacking of pentagonal dodecahedra in (a) melanophlogite and (b) dodecasil-3C or zeolite ZSM-39

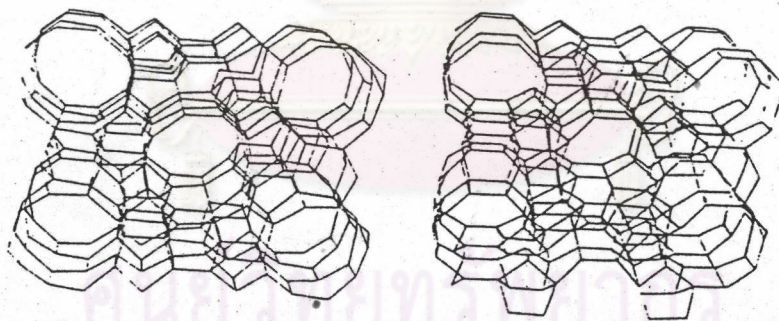
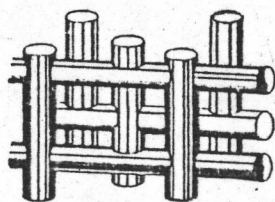
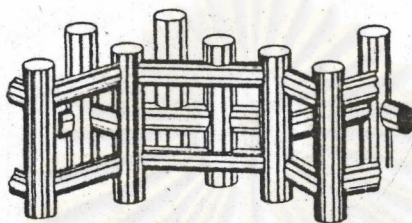


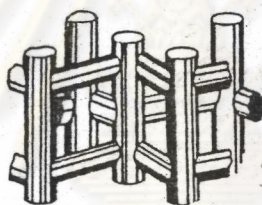
Figure 2.18 Frameworks of ZSM-5 (l.h.s.) and ZSM-11 (r.h.s.)



(a)



(b)



(c)

Figure 2.19 Formal representation of channel patterns in
(a) ZSM-11, (c) ZSM-5 and (b) an intermediate structure

จุฬาลงกรณ์มหาวิทยาลัย

2.19b). These channels have minimum free dimensions from 5.1 to 5.6 Å, by contrast with the largest windows in melanophlogite or dodecasil-3C of 2.6 Å at most.

Table 2.3, with the exception of kehoeite, refers only to silica and aluminosilicates. AlPO_4 can crystallise in forms isostructural with quartz, tridymite and cristobalite and in addition, using organic bases as templates, a number of other AlPO_4 species have been made which include a structural analogue of sodalite and of erionite/offretite. Analogues of zeolites are known in which Ga replaces Al and Ge replaces Si. Table 2.3 is not intended to include such materials.

2.3 Natural Zeolites

Zeolite minerals have been used in many investigations of zeolite structure and properties (adsorption, ion exchange, etc.). The occurrence of zeolites is somewhat paradoxical. Some minerals which occur extensively are not suitable for most known commercial applications (for example, analcime and phillipsite). Some synthetic zeolites which have extensive commercial use do not have mineral relatives. Other zeolite minerals occur in miniscale quantities; for research purposes, investigators have sometimes been required to work with milligram quantities.

The naming of minerals is thoroughly discussed by Fleischer and McConnell. There may be some question concerning a few minerals such as herschelite (as distinguished from chabazite) and stellerite (as distinguished from stibite). Because of property differences (chemical composition, dehydration behavior, gas adsorption) we have chosen to designate herschelite and stellerite as separate minerals.

Until recently, the nomenclature for zeolite minerals has been confused. Early identifications were based on chemical composition, optical properties, morphology, etc. With the advent of x-ray

crystallography, some zeolite names have been discredited.

2.3.1 Formation Processes and Geologic Occurrence

Most zeolite occurrences in nature are assignable to six types of geologic environments or hydrological systems: [5] saline, alkaline lakes, [6] saline, alkaline soils and land surface, sea-floor sediments percolating water in an open hydrologic system, [7] hydrothermal alteration, and burial diagenesis or metamorphism. Iijima lists two additional geological occurrences; magmatic zeolites and zeolites forming in impact craters.

Zeolites commonly form by direct precipitation from pore fluids as in magmatic and some hydrothermal occurrences or by the alteration of volcanic glasses or poorly crystalline silicate minerals. The most common parent materials are volcanic glass, clays, montmorillonite, plagioclase, nepheline, biogenic silica, and quartz. Under the proper conditions, one zeolite species may replace another species. Temperature, pressure, chemical activity of ionic species, and the partial pressure of water all affect which species of zeolite forms. Temperatures of formation can range from ambient to 700° C, and pressures can range from 1 to 1,000 atm [11, 33].

Figure 2.20 from Hay [15] depicts the modes of occurrence of natural zeolites and the approximate depths at which these zones may be found.

Zone A in fig. 2.20 is characterized by nonalcaline, alkali-rich zeolites, zone B by analcime or heulandite, and zone C by K-feldspar in A, B, C and D and by albite with or without laumontite in E and F.

Saline, Alkaline Lakes

Saline, alkaline lake environments are associated with two types of tectonic settings in arid and semiarid regions: block-faulted

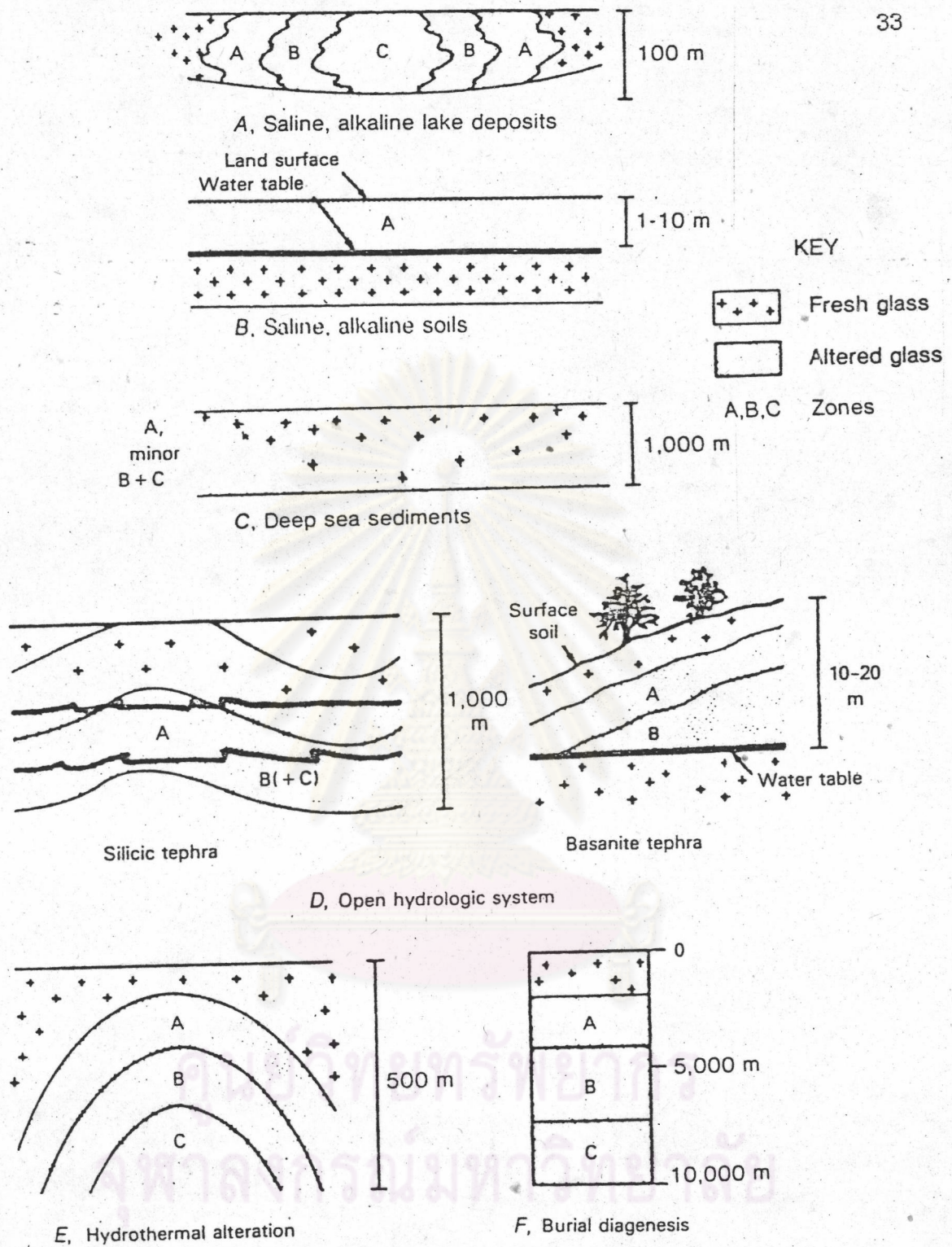


Figure 2.20 Patterns of authigenic zeolites and feldspars

terrains and trough valleys associated with continental rifting . These settings establish a closed basin system and control the transport of clastic material beyond the basin edges. Both are essential for controlling lake chemistry [32, 33].

The restricted lakes in which zeolites form are alkaline, with pH values of 9.5 . Analcime, clinoptilolite, phillipsite, erionite, chabazite, and mordenite commonly form replacing volcanic glass, biogenic silica, poorly crystallized clay, montmorillonite, plagioclase, nepheline, and quartz . These deposits are zoned laterally, as in fig. 2.20 A representing the changing chemistry of the water as evaporation and precipitation of minerals proceed.

The zonation of the mineral beds in the various saline, alkaline lakes indicates the sequence of the zeolite diagenesis [15]:

1. Glass \longrightarrow alkalic, silicic zeolites
2. Alkalic, silicic zeolites \longrightarrow analcime
3. Analcime \longrightarrow K-feldspar
4. Alkalic, silicic zeolites \longrightarrow K-feldspar

Some controlling chemical parameters during the glass to zeolite reactions are the cation ratios, silicon aluminum ratios, and the activity of the water. Dissolution of the glass is controlled by the salinity and pH [15]. These reactions can be rapid, with vitreous tuffs altering to zeolites in less than 1,000 yr . Ancient Lake Tecopa, shown in fig. 2.21, is typical of the saline, alkaline lake environment.

Saline, Alkaline soils

Climate is the controlling factor in the formation of zeolites in saline, alkaline soils. These deposits form in arid and semiarid regions where evaporation causes sodium carbonate-bicarbonate to concentrate in the surface soils Rainwater percolating through the

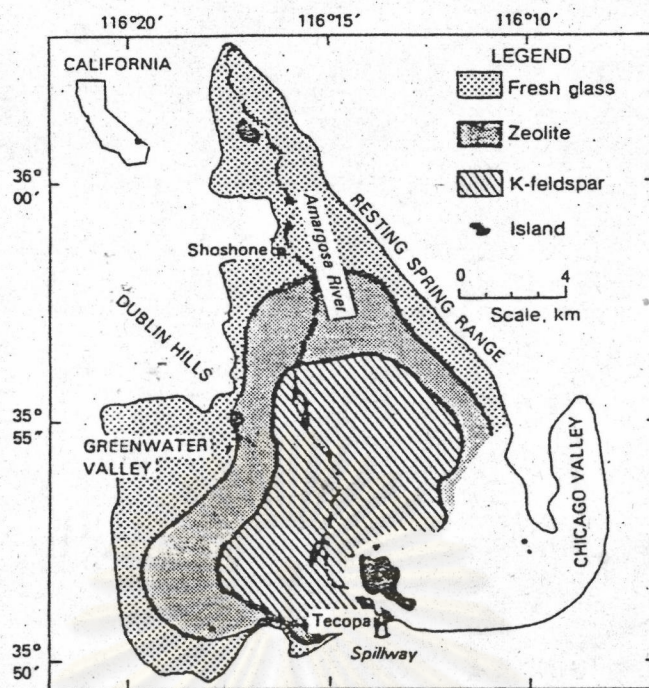


Figure 2.21 Ancient Lake Tecopa near Shohone, CA, showing diagenetic facies

Mineral species	Zone	Zone	Zone III		Zone
	I	II	a	b	IV
"Silicic glass"	■				
Alkali clinoptilolite	■	■			
Clinoptilolite-Ca		■			
Alkali mordenite		■			
Mordenite-Ca		■			■
Analcime		■			
Heulandite		■			
Laumontite				■	
K-Feldspar		■			■
Albite from analcime					■
Albitized plagioclase					■
Opal-Ct	■				
Quartz		■			
Montmorillonite			■		
15A-14A mixed layer			■		
Chlorite			■		
Illite			■		
Prehnite					■
Pumpellyite					■

Figure 2.22 Zonal distribution of zeolites and silicates in burial diagenesis

soils dissolves the sodium carbonate-bicarbonate and increases in pH, allowing it to alter glasses and aluminosilicates present in the soil. The water table is the probable limit of zeolitic alteration processes. Zeolite deposits of this type can approach 18 m in thickness and contain 15% to 40% zeolites. Analcime is the most common zeolite forming in these formations [15]. Minor amounts of phillipsite, natrolite, and chabazite also occur. Deposits of this nature have been observed in the Olduvai Gorge, Tanzania and other sites in Africa and in the Western United States.

Marine Sediments

Zeolites form in marine sediments under low temperatures and moderate pH conditions (pH conditions values of 7 to 8). Zeolites in the slow sedimentation regions of the Pacific and Indian Oceans occur in post-Miocene brown clays, vitric siliceous and calcareous oozes, and basaltic volcanic sediments. Phillipsite is the dominant species. Those in the rapid sedimentation regions of the Atlantic and Pacific margin are in calcareous sediments and terrigenous clays of Paleogene and Cretaceous ages. Clinoptilolite is the dominant species here. Analcime, chabazite, erionite, laumontite, gmelinite, natrolite, and thomsonite also may be present in these marine deposits.

Zeolites in sea-floor sediments form by the reaction of glasses with pore water. Except for the silica content, which ranges from 4 to 65 ppm, sediment pore water is similar to seawater in composition [15]. Phillipsite is associated with the low silica concentrations (less than 20 ppm) typical of basaltic tephtras, and clinoptilolite is associated with the high silica concentrations (20-40 ppm) of siliceous tephtras [15]. Clinoptilolite occurring with phillipsite probably forms when basaltic glass reacts with silica-rich pore waters.

Boles and Wise suggest that since marine clinoptilolite occurs as euhedral crystals, their formation must have been from pore water rather than as a direct replacement of earlier phases. In spite of this, they think that because phillipsite is found in the younger sediments it is likely that the clinoptilolite in the older sediments replaced it and that time was an important factor.

Open hydrologic Systems

Zeolites in open systems form from the percolation of ground water through porous pyroclastic materials rich in reactive glass reacts with the vitric ash, until zeolites are precipitated [15]. Movement of the ground water downward through the system results in a vertical zonation of water composition and authigenic minerals, including zeolites [15]. Typically a silicic tephra may contain an upper zone of fresh glass, montmorillonite, and opal. The next bed can contain up to 90% clinoptilolite, and the underlying zone may contain analcime, potassium, feldspar, and quartz. Alternation of the glass can occur rapidly because of the high pH (approximately 9.5) resulting from hydrolysis [15].

An example of an open-system deposit is the basanite vitric tuffs of Koko Crater in Hawaii [15]. These tuffs consist of 1.5 to 12 m of fresh glass, opal, and montmorillonite. the next lower zone consists of 1.5 to 10 m of palagonite tuffs with phillipsite and chabasite. The lowest zone is 8 m thick and predominantly analcime [15].

Hydrothermal Systems

Zeolites precipitate in hydrothermal systems from alkaline to weakly acidic hot water. The assemblages observed are controlled by temperature, host rock composition, host rock permeability, and geothermal fluid composition. Clinoptilolite and mordenite occur in the shallowest and coolest zones. Analcime or heulandite and laumontite

or wairakite, the less hydrated forms, occur in the deeper and hotter zones [32, 33]. Submarine hydrothermal activity may be responsible for the formation of some zeolites in deep-sea sediments [16].

Examples of hydrothermal zeolite deposits are found in Yellowstone Park, WY; Wairakei, New Zealand; and Onikobi, Japan. At the Onikobi site in Japan, there are four zones: a mordenite zone, a laumontite zone, a laumontite-wairakite zone, and a wairakite zone.

Burial Diagenetic Systems

Zeolites associated with burial diagenesis occur in thick volcanoclastic sediments that were metamorphosed at increased temperatures. Two reaction sequences are recognized, the alkali zeolite reaction series and the calcic zeolite reaction series. The alkali series includes the zeolites clinoptilolite, mordenite, and analcime. The calcic series includes clinoptilolite, heulandite, and laumontite. Burial diagenetic sequences are typified by vertical zonation. This mineralogical zonation is related to increasing burial depth. Iijima [16] recognized five zones based on the mineralogy of marine sediments subjected to burial diagenesis (fig. 2.22). Temperatures increase with depth, as in the Green Tuff region in Japan where temperatures were 41° to 49° C at the top of the zeolite sequence and 120° to 124° C at the base of the sequence. More hydrated zeolites occur at shallower depths [15]. The upper zones of burial diagenetic sequences are mineralogically similar to open hydrologic systems. The major distinction is the gradual change between zones in the burial diagenetic sequence, compared with the sharp contacts of the open system deposit.

An example of burial diagenetic deposits is the Green Tuff region of Japan [15]. In the Niigata oilfield, the upper zone is 0.8 to 1.9 km thick, containing fresh glass. The next zone, 1.6 to 2.5 km

thick, contains mordenite and clinoptilolite. This is followed by an analcimic zone, 1 km thick, and an albitic zone, 0.7 km thick. Analcime is pseudomorphic after mordenite and clinoptilolite. Temperatures range from 41° to 124° C.

Magmatic Systems

Zeolites crystallize during the late stages of formation of magmatic rocks [3]. They commonly occur as fine crystals lining vugs in basic igneous rocks, although they also occur as interstitial grains and globules. Crystalline zeolites form through interaction of fluids with the surrounding rock. Zeolite globules form when water rich magma separates into two immiscible liquids.

The zeolites that form under magmatic conditions are grouped by bulk composition. Aluminum-rich zeolites occur in basic igneous rocks with low silicon-to-aluminum ratios. Aluminum-poor zeolites occur in igneous rocks richer in silicon. Several zeolites that occur in igneous rocks are analcime, clinoptilolite, heulandite, mesolite, mordenite, natrolite, phillipsite, and stilbite.

Impact Craters

Iijima [3] reports zeolites occurring in the Nordlinger Ries impact crater in West Germany. In this occurrence, glass formed by the meteor impact altered to analcime and smectite. Microcavities in the deposits were filled by analcime, clinoptilolite, erionite, harmotome, and phillipsite.

2.3.2 Exploration

Extensive exploration for natural zeolite deposits did not begin until the 1950's, when Union Carbide Corp., through its Linde Division, initiated a search for minable quantities of natural zeolites that might compete with their synthetic zeolites [3]. In describing the onset of this project. Mumpton [3] reports that mineralogical and mineral commodity consultants employed by Union Carbide did not believe

that minable deposits of zeolites would be found. They, like most researchers, believed that zeolites were mineralogical curiosities that filled vugs and fractures in igneous rocks. However, in the 5-yr effort, over 3,000 samples were collected and approximately 200 new zeolite occurrences in volcanoclastic sedimentary rocks were discovered.

As the initial search was going on, a thorough literature search revealed earlier discoveries of sedimentary deposits. Coombs[3] at the University of Otago in New Zealand, described the widespread occurrence of laumontite, analcime, and heulandite in burial metamorphic sequences of pyroclastic sediments in that country and demonstrated the occurrence of substantial amounts of zeolites in "nonigneous" environments. Ames, Sands, and Goldich also described large occurrences of clinoptilolite at Hector, CA. This information prompted Union Carbide's Linde Division to intensify its investigation of zeolite occurrences in pyroclastic rocks.

Samples from the Hector deposit were examined by standard X-ray diffraction and microscopic techniques [3]. Mumpton reported that "several fine-grained, homogeneous, lightweight samples from the Hector deposit, representing beds as thick as 12-15 ft. were found to contain as much as 80-85% clinoptilolite" and that "the Hector samples demonstrated conclusively that nearmonomineralic deposits of natural zeolites could indeed be found in mineable quantities within the continental United States. They also demonstrated that the few reports in the earlier geological literature about the occurrence of zeolites in sedimentary rocks of volcanic origin were not flukes, but that many more such deposits were likely to be found in geologically similar environments throughout the western part of the country and probably throughout the world [3]."

Early in 1958, a sample described as erionite from a

million-short-ton, easily mined, sedimentary deposit was submitted to Linde [3]. Laboratory examination indicated that the sample contained 85% to 90% erionite and that its chemical, adsorption, optical, and X-ray diffraction properties closely matched those of Linde's synthetic analog, zeolite T. Later, the Kennedy Minerals Co., discoverer of the deposit, revealed that the deposit was located in a broad basin of lacustrine and fluvial sediments about 2 miles west of Rome, OR. Here, the Owyhee River had cut through plateau basalts to expose several hundred feet of volcanogenic sedimentary rocks.

The Linde exploration program remained active until 1961. As it tapered off, Shell Development Co. started a modest exploratory effort led by H.D. Curry [3]. Regnier at Columbia University, described beds of high-grade erionite, clinoptilolite, and an unidentified zeolite (later identified as phillipsite) in altered Cenozoic strata in Pine Valley, NV. Deffeyes reported that these same zeolites had been recognized in near-monomineralic beds of altered tuff in Jersey and Reese River Valleys, NV, and that zeolites seemed to be common in the rocks of the Rocky Mountain west. Zeolites had not been previously recognized in these rocks because of their extremely fine-grained nature (1 to 5 μm) and the tendency of the field geologist and stratigrapher to limit their laboratory studies of these materials to microscopic examinations [35]. Once X-ray diffraction techniques were employed, the presence of zeolites became much more widely recognized in Cenozoic volcanogenic sediments.

Table 2.4 from Mumpton [3] lists the discovery dates of 32 prominent natural zeolite deposits. Nearly 90% were discovered between 1957 and 1962.

The list of 34 zeolite minerals in table 2.5 is based on defining properties such as structure and composition. The minerals are

Table 2.4 Discovery and/or initial commercial investigation of prominent zeolite deposits in the United States

Occurrence	Zeolite	Year	Occurrence	Zeolite	Year
Alabama: Campbell	Clinoptilolite	1965	Nevada—Continued		
Arizona:			Lovelock	Clinoptilolite	1959
Bowie	Chabazite	1959		Ferrierite	1966
	Clinoptilolite	1959		Mordenite	1959
	Erlonite	1959	Pine Valley	Erlonite	1957
	Chabazite	1961			1958
Dripping Springs Valley (Christmas).			Pine Valley (Clay Mounds)	Phillipsite	1957
Horsehoe Dam	Clinoptilolite	1961			1958
Union Pass	Mordenite	1960	Reese River Valley	Chabazite	1958
Wellton	Clinoptilolite	1962			1959
Wikieup	Analcime	1928		Clinoptilolite	1958
	Clinoptilolite	1958		Erlonite	1957
	Phillipsite	1959		Clinoptilolite	1962
California:			New Mexico: Buckhorn		
Barstow (Rainbow Basin)	Analcime	1959	Oregon:		
	Clinoptilolite	1959	Durkee	Chabazite	1970
	Phillipsite	1959		Clinoptilolite	1970
Death Valley Junction	Clinoptilolite	1973		Erlonite	1958
Hectordo	1957	Harney Lake (Narrows)	Clinoptilolite	1959
Shoeshone (Lake Tecopa)	Analcime	1959		Erlonite	1959
	Clinoptilolite	1959		Mordenite	1959
	Erlonite	1959	Rome	Erlonite	1957
	Phillipsite	1959		Mordenite	1962
	Clinoptilolite	1970	Sheaville	Clinoptilolite	1958
Colorado: Creede		{ 1970	South Dakota: Pine Ridge	..do	{ 1958
		1977	Reservation.		{ 1961
Idaho: Castle Creekdo	1961	Texas:		
Nevada:			Marfado	1962
Ash Meadowsdo	1960	Tildendo	1964
Eastgate	Erlonite	1958			
	Mordenite	1962	Utah: Cove Fortdo	{ 1979
Fish Creek Mountains	Clinoptilolite	{ 1957			{ 1980
		1958	Wyoming:		
Hungry Valley	Chabazite	1960	Beaver Divide	Chabazite	1966
	Clinoptilolite	1960		Clinoptilolite	1957
Jersey Valley	Erlonite	{ 1957		Erlonite	1958
		1958	Fort LeClède (Washakie Basin) ..	Clinoptilolite	{ 1973
					{ 1977

Table 2.5 Alist of Zeolite Minerals

Name	Structure Group	Year Discovered	Typical Occurrence in Igneous Rocks	Examples of Occurrence in Sedimentary Rocks
Analcime	1	1784	Ireland, New Jersey	Extensive; Wyoming, etc. Deep sea floor
Bikitaite	6	1957	Rhodesia	
Brewsterite	7	1822	Scotland	
Chabazite	4	1772	Nova Scotia, Ireland	Arizona, Nevada, Italy
Clinoptilolite	7	1890	Wyoming	Extensive; Western U. S., Deep sea floor
Dachiardite	6	1905	Elba, Italy	
Edingtonite	5	1825	Scotland	
Epistilbite	6	1823	Iceland	
Erionite	2	1890	Rare, Oregon	Nevada, Oregon, U.S.S.R.
Faujasite	4	1842	Rare, Germany	
Ferrierite	6	1918	Rare, British Columbia, Italy	Utah, Nevada
Garronite	1	1962	Ireland, Iceland	
Gismondine	1	1816	Rare, Italy	
Gmelinite	4	1807	Nova Scotia	
Gonnardite	5	1896	France, Italy	
Harmotome	1	1775	Scotland	
Herschelite	4	1825	Sicily	Arizona
Heulandite	7	1801	Iceland	New Zealand
Kelwoite	1	1893	Rare, South Dakota	
Laumontite	1	1785	Nova Scotia, Faroe Islands	Extensive; New Zealand, U.S.S.R.
Levynite	2	1825	Iceland	
Mesolite	5	1813	Nova Scotia	
Mordenite	6	1864	Nova Scotia	U.S.S.R., Japan, Western U.S.
Natrolite	5	1758	Ireland, New Jersey	
Offretite	2	1890	Rare, France	
Paulingite	1	1960	Rare, Washington	
Phillipsite	1	1824	Ireland, Sicily	Extensive, Western U.S., Africa, Deep sea floor
Scolecite	5	1801	Iceland, Colorado	
Stellerite	7	1909		
Stilbite	7	1756	Iceland, Ireland, Scotland	
Thomsonite	5	1801	Scotland, Colorado	
Viscite	1	1942	Rare, Belgium	
Wairakite	1	1955	New Zealand	
Yugawaralite	1	1952	Japan	

listed in alphabetical order for convenience; also included are the structural group, extent of occurrence, and year of discovery.

2.3.3 Physical Properties

Pure zeolites are colorless; some mineral specimens may be colored because of the presence of finely divided oxides of iron or similar impurities [8]. Synthetic zeolites may be colored due to the introduction of certain types of transition metal ions such as Co^{2+} by ion exchange. The densities of the zeolites range generally between 2 and 2.3 g/cc. The exchange cation does, of course, change the density which primarily depends on the basic framework structure, that is, the openness and void volume. Zeolites which are rich in barium may have higher densities of 2.5 to 2.8 g/cc. Optically, the refractive indices vary between 1.47 and 1.52 with birefringence of 0 to about 0.015. Optical and physical properties of some zeolite minerals are summarized in tables 2.6 (a-e). These properties have been selected as representative properties. In some cases, it is difficult to assign a particular X-ray powder diffraction pattern to a certain species because variations do occur in the X-ray pattern as a result of variation in the exchange cation composition. The table for each mineral includes x-ray powder data which have been obtained from selected sources including the Powder Diffraction File. The intensities of the individual x-ray reflections are those given in the source. In some instances the intensities are given on a relative scale, such as vs, s, ms, m, w, vw and vvw, corresponding to very strong, strong medium strong, medium, weak, very weak and very very weak.

For the identification of zeolites which occur as fine-grained crystals in sedimentary rocks, x-ray diffraction is the primary tool. Routine diffractometer analysis is generally sufficient for identification of zeolites which occur in rock in concentrations of more

Table 2.6a Tables of mineral zeolites data - Analcime

Structure Group:	1
Typical Unit Cell Contents:	$\text{Na}_{16} [(\text{AlO}_2)_{16}(\text{SiO}_2)_{32}] \cdot 16 \text{H}_2\text{O}$
Variations:	$\text{Si}/\text{Al} = 1.8\text{-}2.8; \text{H}_2\text{O}/\text{Al}_2\text{O}_3 = 2\text{-}2.6$
Occurrence:	Igneous and sedimentary rocks; Iceland, Nova Scotia, New Jersey, Wyoming, Arizona, Utah, California, Nevada
System:	Cubic, $a = 13.72 \text{ \AA}$
Habit:	Icositetrahedra, radiating aggregates
Twinning:	[001], [110] lamellar
Cleavage:	[001] poor
Density:	2.24-2.29
Hardness:	5½
Optical Properties:	Isotropic, $n = 1.479\text{-}1.493$; birefringence, $\delta = \text{slight}, < 0.001$
Reference:	3-6, 38-40

X-Ray Powder Data

hkl	d(A)	I	hkl	d(A)	I	hkl	d(A)	I
200 ^a	6.87	< 10	631	2.022	10	842	1.498	20
211	5.61	80	543	1.940	< 10	761	1.480	20
220	4.86	40	640	1.903	50	664	1.463	10
321	3.67	20	633	1.867	40	754	1.447	10
400	3.43	100	642	1.833	< 10	932,	1.415	40
332	2.925	80	732,	1.743	60	763		
422	2.801	20	651			941,	1.386	<10
431	2.693	50	800	1.716	30	853		
521	2.505	50	741	1.689	40	860	1.372	10
440	2.426	30	820	1.664	10	1011	1.359	40
611,	2.226	40	822,	1.618	20	1031	1.308	10
532			660			871	1.285	20
620	2.168	< 10	831,	1.596	30	1033	1.263	20
541	2.115	< 10	743			963	1.220	30

^a (200) not in agreement with space group Ia3d

Table 2.6b Tables of mineral zeolites data - Chabazite

Structure Group:	4
Other Designation:	Acadialite, Haydenite, Phacolite, Glottalite
Typical Unit Cell Contents:	$\text{Ca}_2 [(\text{AlO}_2)_4 (\text{SiO}_2)_8] \cdot 13 \text{H}_2\text{O}$
Variations:	Na and K; $\text{Ca} > \text{Na}, \text{K}$; $\text{Si}/\text{Al} = 1.6-3$; $\text{Si}/\text{Al} = 3.2-3.8$ reported in sedimentary mineral
Occurrence:	Ireland, Nova Scotia, Colorado; sedimentary in Italy, Africa, Arizona, California, Nevada
System:	Trigonal, $a = 9.42$ $\alpha = 94^\circ 28'$ Hexagonal, $a = 13.78$, $c = 15.06$
Habit:	Rhombohedral
Twinning:	[0001] penetration
Cleavage:	[1011]
Density:	2.05 - 2.10
Hardness:	4½
Optical Properties:	Uniaxial (-), $\epsilon = 1.48-1.50$, $\omega = 1.480-1.50$; birefringence, $\delta = 0.002-0.005$ mean index 1.46-1.47 in sedimentary chabazite
Reference:	3, 4, 6, 38, 45-48

X-Ray Powder Data

hkl	d(A)	I	hkl	d(A)	I	hkl	d(A)	I
101	9.351	50	311	3.235	6	501	2.358	2
110	6.894	10	204	3.190	5	413	2.310	3
102	6.384	5	312	3.033	2	330	2.300	4
201	5.555	9	401	2.925	100	502	2.277	1
003	5.021	30	214	2.890	30	421	2.233	1
202	4.677	6	223	2.842	3	306	2.123	2
211	4.324	76	402	2.776	4	107	2.119	2
113	4.044	1	205	2.690	7	333	2.090	6
300	3.976	2	410	2.605	10	504	2.016	1
212	3.870	28	322	2.574	2	217	1.941	1
104	3.590	23	215	2.507	11	520	1.911	3
220	3.448	13	116	2.361	2	505	1.871	3

จุฬาลงกรณ์มหาวิทยาลัย

Table 2.6c Tables of mineral zeolites data - Clinoptilolite

Structure Group:	7
Typical Unit Cell Contents:	$\text{Na}_6 [(\text{AlO}_2)_6(\text{SiO}_2)_{30}] \cdot 24 \text{H}_2\text{O}$
Variations:	$\text{Na, K} \gg \text{Ca, Mg; Si/Al} = 4.25\text{-}5.25$; in sedimentary type $\text{Si}/(\text{Al} + \text{Fe}^{3+}) = 4.1\text{-}5.6$
Occurrence:	Wyoming; extensive sedimentary occurrences in western U. S.
System:	Monoclinic, $a = 7.41$ $b = 17.89$ $c = 15.85$ $\beta = 91^\circ 29'$
Habit:	Tabular, platy
Cleavage:	[010]
Density:	2.16
Optical Properties:	Biaxial (-), $\alpha = 1.476$, $\beta = 1.479$, $\gamma = 1.479$
Reference:	6, 38, 49-53

X-Ray Powder Data

hkl	d(A)	I	hkl	d(A)	I	hkl	d(A)	I
020	8.92	100	004	3.964	55	222	3.168	14
002	7.97	3	042	3.897	57	222	3.119	15
10 $\bar{1}$	6.78	2	14 $\bar{1}$	3.74	7	231	3.07	8
031	5.61	2	21 $\bar{1}$	3.55	6	044	2.974	80
112	5.15	7	051	3.48	3	035	2.793	15
130	4.65	14	114			12 $\bar{5}$	2.793	15
10 $\bar{3}$	4.35	2	220	2.419	16	16 $\bar{1}$	2.728	33
132	3.964	55	202	3.324	4			

ศูนย์วิทยทรัพยากร
จุฬาลงกรณ์มหาวิทยาลัย

Table 2.6d Tables of mineral zeolites data - Ferrierite

Structure Group:	6
Typical Unit Cell Contents:	$\text{Na}_{1.5}\text{Mg}_2[(\text{AlO}_2)_{5.5}(\text{SiO}_2)_{30.5}] \cdot 18 \text{H}_2\text{O}$
Variations:	Na, K in Nevada ferrierite Less Mg in Agoura ferrierite
Occurrence:	Kamloops, British Columbia, Vicenza, Italy; Agoura, California; sedimentary in Nevada.
System:	Orthorhombic, $a = 19.16$ $b = 14.13$ $c = 7.49$
Habit:	Blades, needles
Cleavage:	[100]
Density:	2.136-2.21
Hardness:	3 - 3½
Optical Properties:	Mean index = 1.484 in Na, K ferrierite; biaxial (+), $\alpha = 1.478$, $\beta = 1.479$, $\gamma = 1.482$; birefringence, $\delta = 0.004$, $2V\gamma = 50^\circ$
Reference:	38, 52, 67 - 70

X-Ray Powder Data

hkl	d(A)	I	hkl	d(A)	I	hkl	d(A)	I
110	11.33	20	112,	3.54	80	350,	2.58	30
200	9.61	100	040			042,		
020,	7.00	30	202	3.49	80	701		
101			501	3.42	20		2.49	20
011	6.61	20	240	3.31	20		2.43	20
310	5.84	50	600	3.20	10		2.37	40
121	4.96	10	141,	3.15	30		2.32	10
301,	4.80	10	312				2.26	10
400			521,	3.07	30		2.11	20
130	4.58	10	431				2.04	20
321,	3.99	90	530	2.97	30		2.00	30
031			620,	2.90	20		1.94	30
411	3.88	10	132				1.87	30
330,	3.79	20	422	2.72	20		1.78	40
510	3.69	50						

Table 2.6e Tables of mineral zeolites data - Faujasite

Structure Group:	4							
Typical Unit Cell Contents:	$\text{Na}_{12}\text{Ca}_{12}\text{Mg}_{11}[(\text{AlO}_2)_{59}(\text{SiO}_2)_{133}] \cdot 235 \text{H}_2\text{O}$							
Variations:	Si/Al = 2.1-2.3, also some K							
Occurrence:	Kaiserstuhl, Germany; reported in Oahu, Hawaii							
System:	Cubic, $a = 24.67$							
Habit:	Octahedral							
Cleavage:	[111]							
Density:	1.91							
Hardness:	5							
Optical Properties:	Isotropic, $n = 1.48, 1.471$							
Reference:	3, 38, 48, 66							
X-Ray Powder Data								
hkl	d(A)	I	hkl	d(A)	I	hkl	d(A)	I
111	14.418	100	533	3.779	32	751,	2.860	22
220	8.784	9	444	3.580	2	555		
311	7.487	5	711,	3.468	5	840	2.767	5
222	7.173	2	551			911,	2.719	3
331	5.695	30	642	3.311	16	753		
422	5.062	1	731,	3.227	5	664	2.641	7
333,	4.772	13	553			931	2.600	4
511			733	3.025	6	10,2,2	2.382	5
440	4.387	32	822,	2.919	10	666		
620	3.915	4	660			880	2.189	3

ศูนย์วิทยทรัพยากร
จุฬาลงกรณ์มหาวิทยาลัย

than 10%. In order to identify zeolites which are present in less than this amount, some method of concentration is necessary. Although special optical data may be reasonably sufficient to identify a larger zeolite crystal of the igneous zeolites, it generally is a supplement to the modern x-ray method. The refractive index, for example, has been used for distinguishing clinoptilolite from heulandite.

Various other methods have been suggested for identifying zeolites. One is based upon contacting the zeolite with its exchangeable cations with a solution of a salt whose cation is excluded by the zeolite due to size. The salt used is tetrabutylammonium chloride. The zeolite is first subjected to exchange with silver using silver nitrate. Then the silver exchanged zeolite is treated with a solution of alkylammonium salt. Because the alkylammonium ion is excluded, the silver ion is removed by precipitation of the insoluble silver chloride. In this event, hydrolysis of the zeolite cation occurs and the solution becomes alkaline. The presence of a zeolite is detected by an increase in pH from about 6 to >9. With other likely ion exchanging minerals such as clays, the pH varies between 6.5 and 7.5 since the large organic cation is exchanged without hydrolysis.

2.4 Synthetic Zeolites

The synthesis of zeolites was first reported by St. Clair Deville in 1862. By heating aqueous solutions of potassium silicate and sodium aluminate in a glass tube at 170°C. Deville produced the zeolite levynite. In 1882, De Schulten reported the synthesis of analcime. However, data are not available to substantiate these and other experiments, and much of the early work cannot be duplicated in the laboratory. The first substantiated synthesis of zeolites was not performed until the 1940's when x-ray diffraction was used to identify phases. Prior to this time, light microscopy was used for phase

identification, and the fine-grained nature of synthesized zeolites made identification difficult.

Early attempts zeolite synthesis sought to duplicate the conditions under which zeolites were through to crystallize in basaltic rocks. In 1959, R.M. Milton and associates at Union Carbide Corp. suggested a new approach, which allowed the synthesis of zeolites at low temperatures. Their method used highly reactive ingredients in a closed system at low temperatures, often below the boiling point of water. This made the large-scale production of synthetic zeolites feasible [5].

2.4.1 Summary List of Synthetic Zeolites

A summary list of the synthetic zeolites is given in table 2.7. This list is presented as an aid in locating information and data concerning any of the synthetic zeolite species.

2.4.2 Mechanism of Zeolite Crystallization

Breck reports the general conditions used in zeolite synthesis:

1. Reactive starting materials such as freshly coprecipitated gels or amorphous solids.
2. Relatively high pH introduced in the form of an alkali metal hydroxide or other strong base.
3. Low-temperature hydrothermal conditions with concurrent low autogeneous pressure at saturated water vapor pressure.
4. A high degree of supersaturation of the components of the gel, leading to the nucleation of a large number of crystals.

The following are simultaneous reactions that occur during the synthesis process :

- Precipitation of a gel phase,
- Dissolution of the gel,
- Nucleation of zeolite(s),

Table 2.7 Alphabetical list of synthetic zeolites

This table is an attempt to sort out the more than 90 species of synthetic zeolites. The zeolites are arranged in alphabetical order either by the letter which indicates the structure type or in some cases by the name of the related mineral where that has been employed in the literature.

The framework structure-type is given in column 2 if known. The cations shown in column 3 indicate the system from which the zeolite crystallizes. For example, zeolite A is synthesized in the sodium form. (Details are given in the Section C which deals with the $\text{Na}_2\text{O} \cdot \text{Al}_2\text{O}_3 \cdot \text{SiO}_2 \cdot \text{H}_2\text{O}$ system.) Zeolite omega, with

the two cations— Na^+ and TMA^+ —is discussed in Section E. The column labeled "Framework" shows the range in Si/Al ratio—when reported—and other framework atoms such as P, Ge, Ga. Column 5 indicates whether or not the zeolite is structurally stable toward the dehydration necessary to determine adsorption properties. The pore size and pore volumes in columns 6 and 7 are determined from adsorption measurements. For added convenience the table containing x-ray powder data is given in column 8. Other designations for the zeolite are shown in column 9 and pertinent literature references in column 10.

Zeolite	Structure Type	Cations	Framework	Stability	Pore Size (Å)	Pore Vol (cc/g)	X-ray Data Table	Other Des.
A	A	Na	Si/Al ~ 1, Ge	Stable	4	0.30	4.27	
N-A	A	Na, TMA	Si/Al = 1.25 - 3	Stable	4.3	0.30	4.28	
P-A ^a	A	Na	Si-Al-P	Stable	4	0.27	4.29	
α	A	Na, TMA	Si/Al = 2 - 3.5	Stable	4.3	0.30	4.30	
Li-A	Unknown	Li	Si/Al = 1	Stable	2.6	0.15	4.31	
Analcime	Analcime	Li	Si/Al = 1.5 - 3.0	Stable	2.6	0.10	—	
B	Gismondine	Na	Si/Al = 1 - 2.5	Struct. contr.	2.6	0.24	4.74	P
Na-B	Analcime	Na	Si/Al = 2	Stable	2.6	—	—	
β	Unknown	Na, TEA	Si/Al = 2.5 - 50	Stable	~6+	0.20	—	
Bikitaite	Bikitaite	Li	Si-Al	—	—	—	—	
P-B ^a	Gismondine	Na	Si-Al-P	Unstable	—	—	4.32	
P-C ^a	Analcime	Na	Si-Al-P	Stable	—	—	4.33	
Clinoptilolite	Clinoptilolite	Li	Si-Al	—	—	—	4.34	
		Ca, Sr, Ba	Si-Al	—	—	—	—	
D	Chabazite	Na, K	Si/Al = 2.3 - 2.5	Stable	4	0.26	4.35	
Ca-D	Wairakite	Ca	Si/Al = 2	—	—	0.11	4.36	
NH ₄ -D	Analcime	NH ₄	Si-Al	—	—	—	—	
Na-D	Mordenite	Na	Si/Al = 5	Stable	4	0.13	4.37	
Rb-D	Z	Rb	Si/Al = 2	—	—	—	—	
Sr-D	Ferrierite	Sr	Si/Al ~ 3.5	Stable	3.5	0.13	4.38	
E	Unknown	Na, K	Si/Al = 1 - 2	Unstable	2.8	0.21	4.59	
Ca-E	Analcime	Ca	Si-Al	—	—	—	4.40	
K-E	Analcime	K	Si/Al = 2	—	—	—	4.41	
TMA-E ^c	Erionite	Na, TMA	Si/Al ~ 3	Stable	—	—	4.42	
F	Unknown	K	Si/Al = 1	Stable	3.6	0.16	4.43	
K-F	Unknown	K	Si/Al = 1	Stable	2.6	0.13	4.92	Z
Sr-F	Gmelinite	Sr	Si-Al	Stable	3.5	0.22	4.44	
Ferrierite	Ferrierite	Na, Ca	Si-Al	—	—	—	4.45	
G	Chabazite	K	Si/Al = 1.15 - 2.7, Ga	Stable	—	0.26	4.46	
P-G ^a	Chabazite	K	Si-Al-P	Stable	—	—	4.47	
Sr-G	Chabazite	Sr	Si-Al	Stable	—	0.28	4.48	
Ba-G	L	Ba	Si/Al = 1.5	Stable	3	0.15	4.49	
Gismondine	Gismondine	TMA	Si/Al = 1.5	—	—	—	—	
H	Unknown	K	Si/Al = 1	Unstable	2.6	0.22	4.50	I
Li-H	Unknown	Li	Si/Al = 4	Stable	2.6	0.16	4.51	
Heulandite	Heulandite	Ca	—	—	—	—	4.52	
HS	Sodalite	Na	Si/Al = 1	—	<2.6	—	4.53	G, Zh
Ca-I	Thompsonite	Ca	Si-Al	—	—	—	4.54	
K-I (see H)								
Sr-I	Analcime	Sr	Si-Al	—	—	—	4.55	
J	Unknown	K	Si/Al = 1 - 1.15	Stable	2.8	0.08	4.56	
Ba-J	Unknown	Ba	Si/Al = 4	—	—	0.10	4.57	
Ca-J	Epistilbite	Ca	Si-Al	—	—	0.19	4.58	

Table 2.7 Alphabetical list of synthetic zeolites (continued)

Zeolite	Structure Type	Cations	Framework	Stability	Pore Size (Å)	Pore Vol (cc/g)	X-ray Data Table	Other Des.
Ba-K	Unknown	Ba	Si-Al	~	-	0.08	4.59	
L	L	K, Na	Si/Al = 2.6 - 3.5	Stable	8	0.20	4.60	
Ca-L	Harmotome	Ca	Si-Al	-	-	-	4.61	
P-L ^a	L	K	Si-Al-P	Stable	6-7	0.14	4.62	
Losod	Losod	Na, C ₈ H ₁₆ N ⁺	Si-Al	Stable	<2.6	0.18	4.63	
M	Unknown	K	Si/Al = 1	Stable	2.6	0.10	4.64	
Ba-M	Harmotome	Ba	Si-Al	-	-	0.13	4.65	
Sr-M	Mordenite	Sr	Si-Al	-	-	-	4.66	
Mordenite	Mordenite	Li	Si-Al	Stable	-	-	4.67	
	Large Port	Na	Si/Al = 5	Stable	7	0.20	4.68	
		Na, Li	Si/Al = 5	Stable	~4	-	4.69	
		Ca	-	Stable	-	-	-	
N	Unknown	Na, TMA	Si/Al = 1	Stable	2.6	0.16	4.70	
Ba-N	Unknown	Ba	Si/Al = 1	Unstable	-	-	4.71	
Natrolite	Natrolite	Na	-	-	-	-	-	
O ^c	Offretite	TMA, K, Na	Si/Al = 3.4 - 4.25	Stable	6	-	-	
Omega ^c	Omega	Na, TMA	Si/Al = 2.5 - 10	Stable	9	0.20	4.72	
Offretite ^c	Offretite	TMA, K, Na	Si/Al = 2.5 - 5	Stable	6	0.15	4.73	
P _c	Gismondine	Na	Si/Al = 1 - 2.5, Ge	Struct. contr.	2.6	0.24	4.74	P-1
P _t	Gismondine	-	Si/Al = 1.5 - 2.5	-	2.6	0.22	4.75	
N-P ^c	Gismondine	Na, TMA	-	-	-	-	-	N-L, N-B
P-(Cl) ^b	ZK-5	Ba	Si/Al = 4.4 - 4.9	Stable	-	-	4.76	
Phillipsite	Phillipsite	Li	-	-	-	-	-	
Q	Unknown	K	Si/Al = 1 - 1.2	Unstable	2.8	0.23	4.77	
Q-(Br) ^h	ZK-5	-	Si/Al = 4.3 - 5.1	Stable	-	-	4.78	
Ca-Q	Mordenite	Ca	Si/Al = 5	-	-	-	-	
Sr-Q	Yugawaralite	Sr	Si/Al = 3	-	-	0.12	4.79	
R	Chabazite	Na	Si/Al = 1.7 - 1.8	Stable	3.5	0.26	4.80	
P-R	Chabazite	Na	Si-Al-P	Stable	3.5	0.19	4.81	
Sr-R	Heulandite	Sr	Si-Al	-	-	-	4.82	
S	Gmelinite	Na	Si/Al = 2.3 - 2.95	Stable	3.5	0.23	4.83	E, Na-S
T	Offretite, Erionite	Na, K	Si/Al = 3.2 - 3.7	Stable	4	0.23	4.84	
Ba-T	Unknown	Ba	Si/Al = 1	Unstable	-	0.06	4.85	
Na-V	Thomsonite	Na	Ga-Si	-	-	-	-	
W	Phillipsite	K	Si/Al = 1.15 - 2.45	Stable	2.8	0.22	4.86	K-M, K-H
P-W ^a	W	K	Si-Al-P	Stable	3.8	0.19	4.87	
X	Faujasite	Na	Si/Al = 1 - 1.5, Ga, Ge	Stable	8	0.36	4.88	R
N-X ^c	Faujasite	Na, TMA	Si/Al = 1 - 1.5	Stable	8	0.36	4.89	
Y	Faujasite	Na	Si/Al = > 1.5 - 3	Stable	8	0.34	4.90	
N-Y ^c	Faujasite	Na, TMA	Si/Al = > 1.5 - 3	Stable	8	0.34	4.91	
Z	Unknown	K	Si/Al = 2	Stable	2.6	0.14	4.92	K-F
Z(Cl) ^b	Like Z	K	-	-	-	-	-	N, O
Z-21	Unknown	Na	Si/Al = 1.7 - 2.1	-	-	0.14	4.93	
ZK-4 ^c	A	Na, TMA	Si/Al = 1.25 - 2.0	Stable	4.3	0.25	4.94	
ZK-5	ZK-5	Na, C ₈ H ₁₈ N ₂ ²⁺	Si/Al = 2 - 3	Stable	4.3	0.27	4.95	
ZK-19	Phillipsite	Na, K	Si/Al = 1.5 - 3.1	Stable	2.6	0.14	4.96	
ZK-20	Levynite	Na, C ₇ H ₁₅ N ₂ ⁺	Si/Al = 2 - 2.5	Stable	3.5	-	4.97	
ZK-21	A	Na, TMA	Si/Al = 1 - 2	Stable	4.3	0.25	4.98	
ZK-22	A	Na, TMA	Si/Al = 2 - 3.5	Stable	4.3	0.25	-	
ZSM-2	Unknown	Li	Si/Al = 1.65 - 2.0	Stable	6	0.22	4.99	
ZSM-3	Faujasite	Na, Li	Si/Al = 1.0 - 3.0	Stable	8	0.30	4.100	
ZSM-4 ^c	Unknown	Na, TMA	Si/Al = 3.0 - 7.5	Stable	6+	0.14	4.101	
ZSM-5 ^d	Unknown	Na, TPA	Si/Al = 2.5 - 50	Stable	6	0.10	4.102	
ZSM-8 ^e	Unknown	Na, TEA	Si/Al = 2.5 - 50	Stable	5	0.10	4.103	
ZSM-10	Unknown	K, C ₈ H ₁₈ N ₂ ²⁺	Si/Al = 2.5 - 3.5	Stable	6+	0.14	4.104	

^a Phosphate zeolite^b Contains a salt, e.g., BaCl₂, BaBr₂^c TMA = tetramethylammonium^d TPA = tetrapropylammonium^e TEA = tetraethylammonium

Continued crystallization and crystal growth of the zeolite(s),

Dissolution of the initial metastable phase(s),

Nucleation of a more "stable" metastable phase or phases,

Continued crystallization and crystal growth of the new crystalline phase(s) while the initial crystals are dissolving,

Dissolution of the equilibrium phase(s),

Nucleation of the equilibrium phase(s),

Crystallization and crystal growth of the final crystalline phases.

When solution of the aluminate and polysilicate anions are mixed to form the hydrous gel, the aluminate anions and silicate anions undoubtedly undergo a polymerization process. The gel structure thus produced is amorphous and in a state of high simplicity. The composition and structure of this hydrous gel is controlled by the size and structure of the polymerizing species. Since the silicate may vary in chemical composition and molecular weight distribution, different silicate solutions may lead to differences in the gel structure. Therefore gelation controls the nucleation of the zeolite crystallites. The crystal size and morphology of zeolites grown from gels generally appear to support this. The crystals are very small, several microns in size, uniform, and often euhedral. The high degree of supersaturation of the ionic species present in the gel must lead to rapid and heterogeneous nucleation and the formation of a large number of nuclei.

The size and charge of the hydrated cation species which serves as a nucleation site for the polyhedral structural unit also influences the nucleation process. The cation is known to have an effect on the silicate and probably on the aluminate species in solution. (The more open zeolite structures appear to be crystallized

from gels which contain sodium as the alkali rather than potassium, the latter leading to less open zeolite structures in general). During the crystallization of the gel, the aluminate and silicate components must undergo a rearrangement in order to form the crystalline structure. This occurs by depolymerization and solubilization of the gel.

A schematic version of the crystallization of an amorphous aluminosilicate gel to a zeolite is given in fig. 2.23. The gel structure, represented in two-dimensions, is depolymerized by the hydroxyl ions which produce soluble aluminosilicate species that may regroup to form the nuclei of the ordered zeolite structure. In this version the hydrated cation acts as a template. The representation presented is for the formation of the zeolite X structure based upon the truncated octahedron unit. A similar scheme could be based on the use of other secondary building units such as the double 6-ring.

Because of the multitude of reactions, time is an important factor determining phase stability and crystal ordering. Breck states "that a mineral zeolite which has existed over long periods of geological time and a synthetic zeolite with a related structure but which was synthesized rapidly in the laboratory may exhibit differences in properties due to the ordering that may occur in the mineral as opposed to the lack of ordering the synthetic structure shows." Many of the synthetic zeolites that are not structurally related to any natural zeolite may be nonequilibrium phases. Metastable synthetic structures may also explain why many natural zeolites do not have synthetic counterparts despite the synthesis of over 100 different zeolite types.

2.5. Methods of Synthesis

The hydrothermal alteration and synthesis of silicates as disclosed in 156 papers published from 1845 to 1937 has been reviewed in an extensive paper by Morey and Ingerson[8]. Those results encompass the

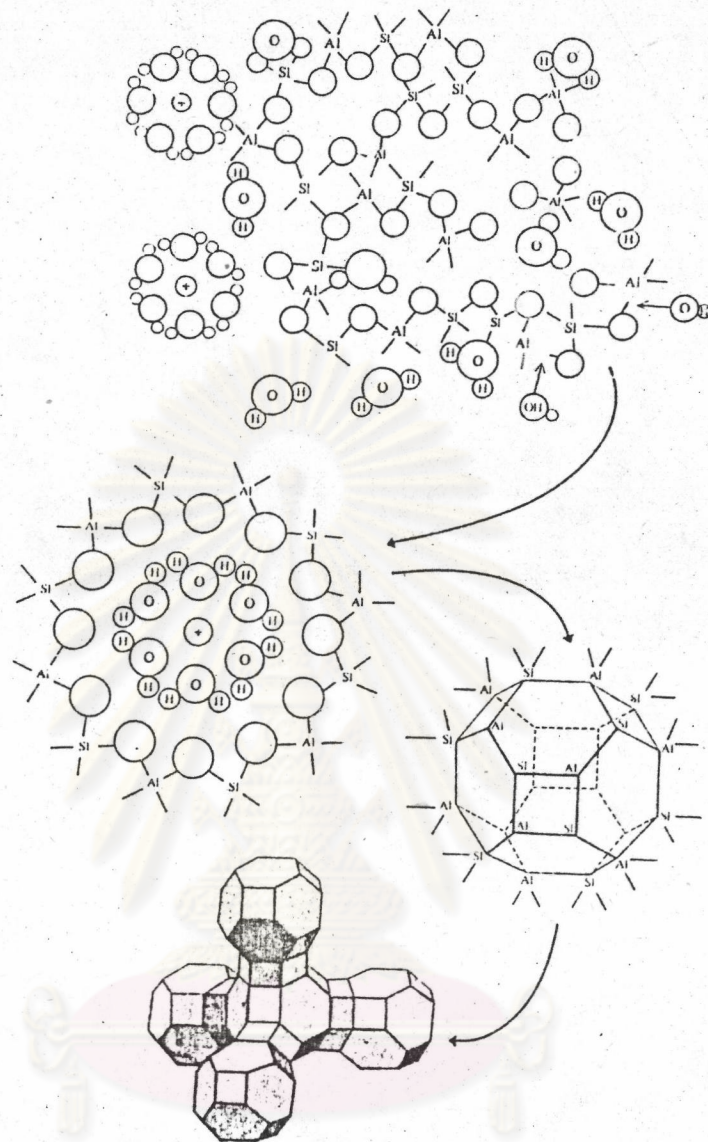


Figure 2.23 Schematic representation of the formation of zeolite crystal nuclei in a hydrous gel. The gel structure, center, is depolymerized by OH^- ions. Tetrahedra regroup about hydrated sodium ions to form the basic polyhedral units

last 100 years and concern the formation of synthetic types of zeolites (table 2.8). Identification of the various products obtained was based upon chemical analysis or optics. Since in most instances the products are very small in particle size, it has been generally concluded that these results are very much in doubt. For example, Baur reported the synthesis of a potassium "faujasite" which was later shown to be the compound K_2SiF_6 . Until identification of polycrystalline materials by means of x-ray powder data became common, positive identification of the products as zeolites was not possible.

Several processes are used to synthesis zeolites as follows:

2.5.1 Y-Zeolite Synthesis [3]

Magee and Blazek discuss the synthesis of zeolite Y using silica gels as a basic ingredient. The procedure they report is as follows:

1. Place 2,090 g H_2O in a resin kettle.
2. Dissolve 162.2 g NaOH in the water.
3. Add 425 g of sodium aluminate, containing 24 wt % Al_2O_3 20 wt % Na_2O , and 56 wt % H_2O .
4. Cool to $100^\circ F$, and then add 570 g of calcined silica.
5. Cold-age at $100^\circ F$ for 24 h with mild agitation.
6. Increase temperature to $212^\circ F$, and age for 24 hr with mild agitation.
7. Quench with water, and filter to remove the solids from the mother liquor.
8. Wash with hot water, and dry in forced-air oven at $250^\circ F$.

This process yields 464 g of sodium-Y zeolite ($Na_2O \cdot Al_2O_3 \cdot 5SiO_2 \cdot nH_2O$). The silicon-aluminum ratio is 2.5 in this process.

2.5.2 ZK-5 Synthesis [8]

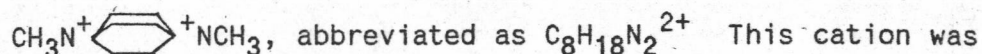
Table 2.8 Selected summary of unsubstantiated zeolite syntheses [8]

<i>Date</i>	<i>Zeolite</i>	<i>Hydrothermal Method</i>	<i>Investigator</i>
1862	Levynite	K silicate + Na aluminate, 170°C	St. Claire Deville
1880	Analcime	Na silicate + Al ₂ O ₃ glass, 180°C	A. de Schulten
1882	Analcime	Na silicate + Na aluminate, 180°C	A. de Schulten
1883	Analcime	SiO ₂ , NaOH solution, Al ₂ O ₃ , 400°C	C. Friedel, E. Sarasin
1885	Analcime	conversion of chabazite, 200°C	J. Lemberg
1887	Analcime	kaolin + Na silicate, 200 - 220°C	J. Lemberg
	Analcime	feldspars + Na ₂ CO ₃ , 200°C	
	Natrolite	scolecite + NaCl	
	Chabazite	feldspars + Na ₂ CO ₃ , 100°C	
1890	Chabazite	recrystallization, 150 - 170°C	C. Doelter
	Heulandite	anorthite + H ₂ O + CO ₂ , 200°C	
	Analcime	Na ₂ O + Al ₂ O ₃ + SiO ₂ + H ₂ O, 100 - 200°C	
	Scolecite	recrystallization	
1894	Natrolite	anorthite, 174 - 177°C	St. J. Thugutt
1896	Thomsonite	muscovite + NaOH, 200°C	G. Friedel
1906	Analcime	nepheline + Na ₂ CO ₃ + H ₂ O, 200°C	C. Doelter
	Natrolite	Na ₂ CO ₃ + Al ₂ O ₃ + SiO ₂ , 90°C	C. Doelter
1911	K Faujasite ^a	K ₂ O, Al ₂ O ₃ , SiO ₂ , 350°C	E. Baur
1916	Analcime	adularia + NaAlO ₂ , 280°C	E. A. Stephenson
1918	Analcime	Na ₂ O, Al ₂ O ₃ , SiO ₂ , 300°C	W. J. Müller, J. Königsberger
1927	Mordenite	feldspars plus carbonates at	R. J. Leonard
	Phillipsite	300 - 500°C in steam at low press.	
1929	Natrolite	paragonite + NaOH, 400°C	E. Gruner
1936	Analcime	Na silicate + Na aluminate, 282°C	F. G. Straub

^aShown to be hieratite, K₂SiF₆.

ศูนย์วิทยทรัพยากร
จุฬาลงกรณ์มหาวิทยาลัย

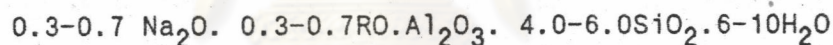
The synthesis of zeolite ZK-5 from sodium aluminosilicate gels was achieved using the dibasic nitrogenous cation.



This cation was introduced in the form of 1, 4-dimethyl-1, 4-diazoniacyclo (2.2.2) octane silicate, which was first prepared from 1,4-diazabicyclo (2.2.2) octane. The composition of the reaction mixtures for the synthesis of ZK-5 have the following mole ratios:

$\text{SiO}_2/\text{Al}_2\text{O}_3$:	4-11
$\text{Na}_2\text{O}/\text{Al}_2\text{O}_3 + \text{C}_8\text{H}_{18}\text{N}_2\text{O}/\text{Al}_2\text{O}_3$:	6-19
$\text{Na}_2\text{O}/\text{Al}_2\text{O}_3$:	1.5-2.3
$\text{H}_2\text{O}/\text{Al}_2\text{O}_3$:	200-700

Alumina was added in the form of sodium aluminate solution, which was then mixed with the quaternary ammonium silicate solution to form a gelatinous amorphous gel. Heating at 100°C for a period of 9 days resulted in the formation of zeolite ZK-5. By analysis the chemical composition of the zeolite is:



where $\text{R} = \text{C}_{18}\text{H}_{18}\text{N}_2^{2+}$

The x-ray powder data are not like any mineral zeolite. Structural analysis confirmed it as a unique zeolite structure.

2.5.3 ZSM-5 Synthesis [4]

This examples illustrates the preparation off zeolite ZSM-5 22.9 grams SiO_2 was partially dissolved in 100 ml 2.18 N tetrapropylmmonium hydroxide by heating to a temperature of about 100°C . There was then added mixture of 3.19 grams NaAlO_3 (comp: 42.0 wt percent Al_2O_3 30.9 wt. percent Na_2O , 27.1 wt. percent H_2O) dissolved in 53.8 ml. H_2O . The resultant mixture had the following composition: 0.382 mole SiO_2 0.0131 mole Al_2O_2 , 0.0159 mole Na_2O , 0.118 mole $[(\text{CH}_2\text{CH}_2\text{CH}_2)_4\text{N}]_2\text{O}$, 6.30 moles H_2O . The mixture was placed in a Pyrex lined autoclave and

heated at 150°C. for six days. The resultant solid product was cooled to room temperature, removed, filtered, washed with 1 liter H₂O and dried at 230°F. A portion of this product was subjected to x-ray analysis and identified as ZSM-5. A portion of the product was calcined at 1000°F. in air for 16 hours.

2.5.4 ZSM-11 Synthesis [17]

Different forms of silica can be used as the silicon source of this invention. The following components were mixed together in a blender in the following sequence:

1. 88 grams of fine colloidal SiO₂ (30 percent)
2. 1.2 grams of sodium aluminate
3. 11 grams of tetra butyl phosphonium chloride
4. 250 grams of H₂O
5. 2.4 grams of NaOH

The mixture appeared as a very dilute colloidal suspension. Crystallization was conducted at 500°F. for 67 hours.

2.5.5 ZSM-34 Synthesis [18]

ZSM-34 was prepared by mixing together the following solutions:

A. Caustic Aluminate

69.89 grams sodium aluminate (20% Na,
43.1% Al₂O₃ and balance H₂O)
29.28 grams NaOH (77.5 wt% Na₂O)
26.4 grams KOH (86.4% KOH)
540 grams H₂O

B. Silica Solution

780 grams Colloidal silica sol. (30% SiO₂)

C. Choline Chloride

228 grams

solution C was added to solution A in a 2 liter autoclave with mixing and then solution 3 was added, followed by a 15 minute continuous mixing. The autoclave was then sealed and heated to and held at 300°F for 8 days. The contents were stirred continuously during the 8 days crystallization period.

The autoclave and its contents were then cooled to room temperature, filtered and washed to separate the crystalline product from the reaction mixture.

2.5.6 Vanadosilicate Catalyst Synthesis [19]

Reagents used and the preparation procedures are shown in table 2.9 and fig. 2.24, respectively. Although the procedures are similar to conventional ones for the preparation of the ZSM-5, some important improvements were made in the present procedures to prepare uniform zeolite crystals: firstly, a gel mixture was prepared by adding 60 ml of solution A-1 and 45 ml of solution B-1 into 208 ml of solution C-1 while maintaining a pH of 9-11 at room temperature and vigorously stirring with an ultra disperser. The precipitate was separated from solution by centrifuge. The precipitated gel mixture was milled for totally one hour by motordrive mortar, Yamato Nitto, UT-21. The milling precipitate and the supernatant of the decant solution were mixed together and charged in an autoclave. The atmosphere in the autoclave was replaced by N₂ with 3 kg/cm² gauge. This was heated from room temperature to 160°C with a constant heating rate, 1.6°C/min, and then up to 210°C with a heating rate of 12°C/hr. The crystals produced were washed with distilled water by using the centrifugal separator until no Cl ions were detected. The crystals were dried at 120°C for 3 hr, and then calcined in an air stream at 540°C for 3.5 h. The calcined crystals were ion-exchanged twice by 1 M NH₄NO₃ solution at 80°C for 1 hr. This was washed with distilled water, dried overnight at 100°C and

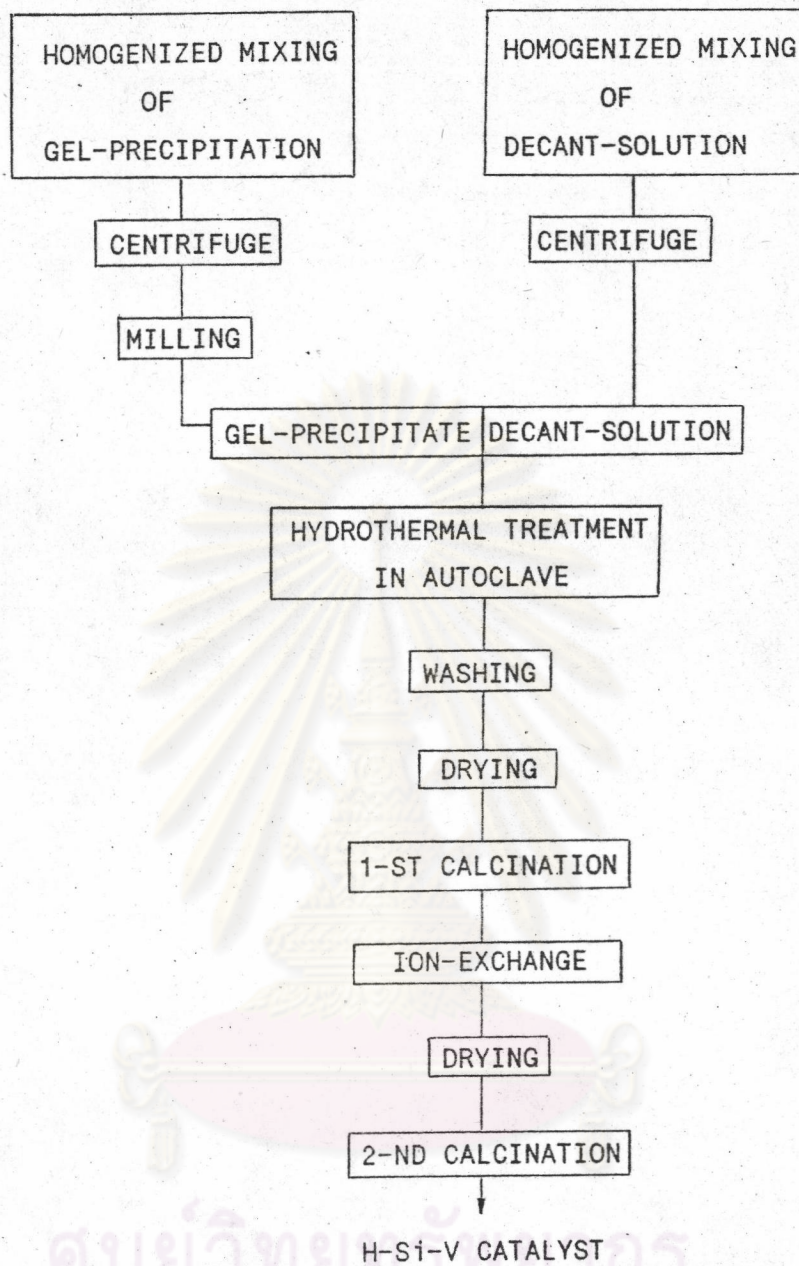


FIGURE 2.24 Procedure of the catalyst preparation [19]

Table 2.9 Reagents for catalyst preparation

Solution for the gel preparation		Solution for the decant-solution preparation	
<u>Solution A-1</u>		<u>Solution A-2</u>	
VCl ₃	x g	VCl ₃	x g
TPABr ^a	5.7 g	TPABr	7.5 g
NaCl	12.0 g	distilled H ₂ O	60 ml
distilled H ₂ O	60 ml	conc. H ₂ SO ₄ (97.0%)	3.4 ml
conc. H ₂ SO ₄	3.4 ml		
<u>Solution B-1</u>		<u>Solution B-2</u>	
water glass ^b	69 g	water glass	69 g
distilled H ₂ O	45 ml	distilled H ₂ O	45 ml
<u>Solution C-1</u>		<u>Solution C-2</u>	
TPABr	2.2 g	NaCl	26.3 g
NaCl	40.6 g	distilled H ₂ O	104 ml
NaOH	2.4 g		
distilled H ₂ O	208 ml		
conc. H ₂ SO ₄ (97.0%)	1.0 ml		

^aTetra-n-propylammonium Bromide, [(CH₃CH₂CH₂)₄N]Br

^bComposed of 9.3% Na₂O, 28.5% SiO₂

^xBased on charged Si/V ratio

ศูนย์วิทยทรัพยากร
จุฬาลงกรณ์มหาวิทยาลัย

then heated in air at 540°C for 3.5 hr. By this preparation method, the charged ratio of Si/V was varied from 40 to infinity by changing VCl_3 in solution A-1 and A-2. The prepared crystallites was tableted and crushed to 7-15 mesh to provide the reaction.

2.6 Physical Characterization of Zeolites

The physical characterization of a material, such as a zeolite begins in principle by visual inspection. This inspection can be refined by the use of instruments which enlarge small particles. Such instruments may be: an ordinary microscope, an electron microscope, or a raster scan electron microscope. Crystalline materials may often be identified by the shape of a crystal which also may give information concerning the presence of crystalline impurities. Furthermore, from the shape of the crystals and their size distribution conclusions may even be drawn which render information concerning the conditions of crystallization or later transformations which will take place, and the colour of the crystals reveals the presence of ionic impurities, such as iron which occurs in natural or industrial zeolites.

In most cases, the structure of the crystalline lattice of the zeolites may be obtained by x-ray diffraction methods. These methods range from simple powder patterns up to sophisticated single crystal methods which allow the localization of all atoms in a unit cell and the calculation of the electron distribution between these atoms.

The x-ray methods may be supplemented by neutron diffraction experiments for the localization of light atoms, especially protons. The neutron scattering experiments may also be used to study.

In addition to the diffraction methods spectroscopic methods are used to study structure problems of zeolites. In this field of study the IR-spectroscopy and recently the ^{29}Si -NMR-spectroscopy has been applied. Strictly speaking, the term "physical characterization" is

applied in zeolite chemistry mostly in connection with the description of special structural elements, responsible for the properties needed in the various applications, e.g. the acid OH-groups in catalysis.

With the IR-spectroscopy a large number of studies has been carried out on the characterization of the strength and the accessibility of the acid OH-groups in different zeolites. The Lewis sites have been characterized by studying the IR-spectra of complexes with sorbed organic bases. Another application of the IR-spectroscopy is the sorption of molecules with different electronic structures on transition metal ions. These types of sorption complexes may also be studied by UV-, visible, or ESR-spectroscopy. Transition metals which are contained in zeolites, incidentally they are used as catalysts in various reactions with hydrogen have been studied extensively by means of Moessbauer-, ESR-, and XPS-spectroscopy.

Furthermore, under the heading of "physical characterization" sorption measurements of any kind have to be summarized, giving information on the heat and entropies of sorption and thus on the interaction of molecules with various shapes and polarity with special structures of the walls of zeolite cavities. The accessibility of the cavities may be studied by diffusion measurement.

2.6.1 Principle of The Characterization of Zeolites by Diffraction Techniques

The most frequently used method for identifying and describing a special zeolite structure, primarily used for patent purposes, is the x-ray powder diffraction method. The reason for this is that this technique is very simple and that zeolites occur mainly as small crystals where single-crystal techniques cannot be applied.

An extended collection of structures described in this way can be found in the book of Breck [8].

In practice, the pattern obtained from Debye-Scherrer-, a Guinier-, or a diffractometer experiment are indexed and the spacings of the obtained (hkl) values are calculated from the angle of the respective peak.

The intensities of the individual x-ray deflections are given in a relative scale using the abbreviations vs, s, ms, m, w, vw, and vvw meaning "very strong", "strong", "medium-strong", "medium", "weak", "very weak", and "very very weak". This is preferentially done when evaluating photographs. When inspecting diffractometer patterns usually the most intense peak is set to be 100 and the others are set relative to this. By this procedure in most cases an identification of the respective zeolite and of the most important impurities can be achieved. If the impurity has at least one strong reflection located at an angle sufficiently far away from the reflections of the main component, impurities occurring only at a few percent can be detected.

The unambiguous identification of a specific zeolite by such a set of powder reflections can sometimes be very difficult, if the structures of several zeolites in question show only slight variations. This has been very impressively shown by Breck [8] comparing the powder diagrams of gismondine, phillipsite, P-zeolite, and some others.

In fig. 2.25 another example is shown which has some importance in the identification of preparations in the ZSM-series for patent applications.

Figure 2.25 depicts the x-ray powder-diffractograms of the two pentasils ZSM-5 and ZSM-8. The difference claimed by the patent applications are connected in the group of reflections which are marked. In the ZSM-5 sample this group consists of reflections which are not very well resolved, whereas for the ZSM-8 this group is very well resolved. A third member of this family shows a systematic extinction

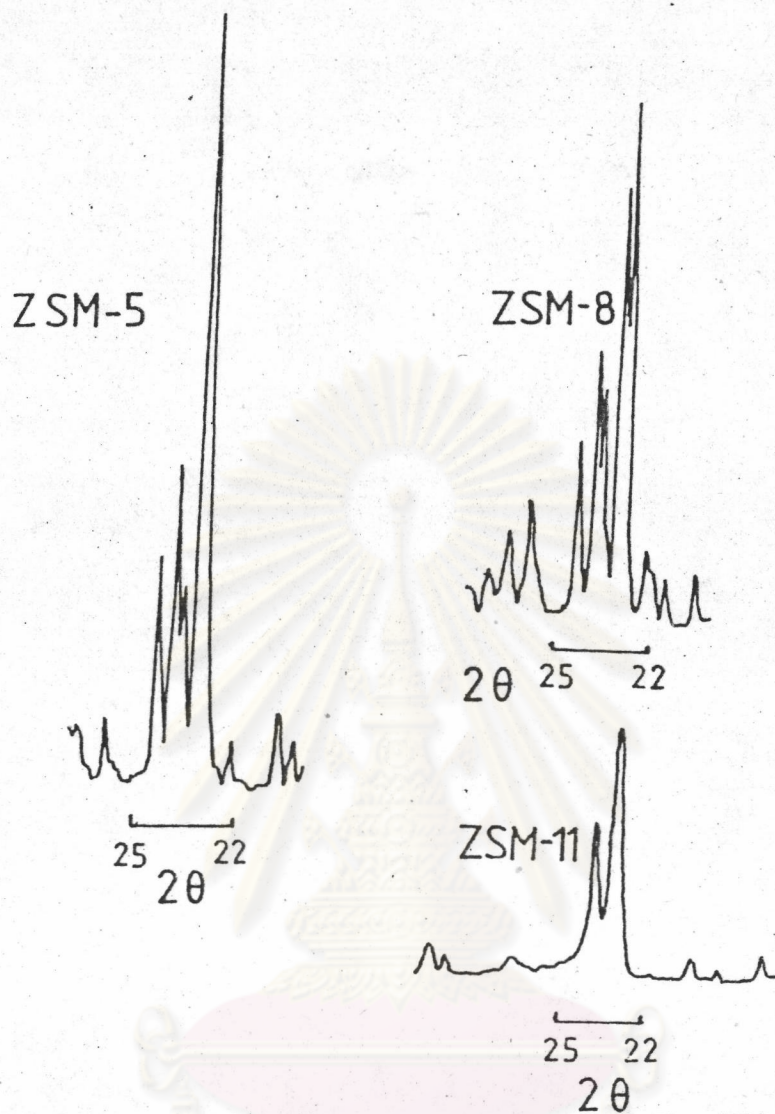


Figure 2.25 X-ray powder diagrams of ZSM-5, ZSM-8, and ZSM-11 around the region of $2\theta=22^{\circ}$ - 25° . ZSM-8 showed a splitting in the highest peak which is not observed for ZSM-5 and ZSM-11. The pattern of ZSM-11 has distinctly fewer lines than the others.

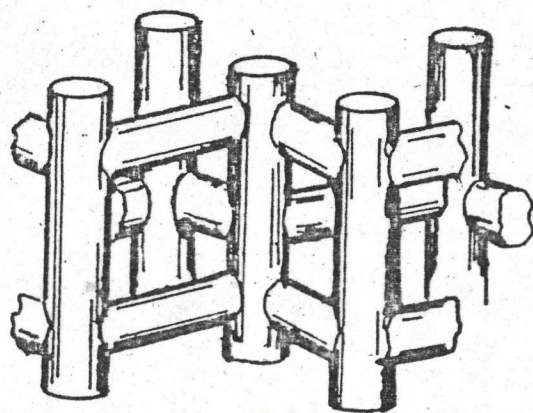
of the $h+k+l = 2n+1$ reflections and a merging of doublets into singlets which give rise to the interpretation that ZSM-11 has a body-centred tetragonal and ZSM-5 an orthorhombic unit cell.

The channel structures which have been determined by Kokotailo et al. [12] are shown schematically in fig 2.26. Whether the ZSM-5 and the ZSM-8 pattern actually belong to different structures is not yet quite clear.

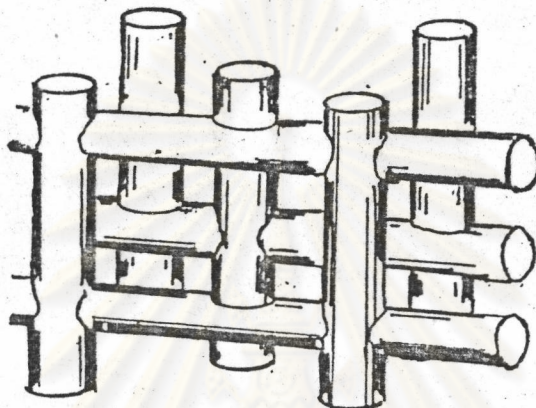
Generally, by inspecting a powder pattern one can try and analyze the given structure. This has been done, particularly for synthetic zeolites with some success. The intensities obtained by the powder patterns may be lost in the background or by an overlapping of reflections so that details concerning the structures, e.g. the exact positions of the cations cannot be resolved. There are several methods reported in the literature for analyzing the peak profiles and to avoid possible disadvantages. One advantage of the powder data is the reduced secondary extinction which disturbs for single crystals, especially the strong reflexes so that in some cases powder data may be used as a supplement to single crystal data.

For an exact determination of the crystal structure single crystals of at least 20-50 μm are necessary and single crystal techniques need to be applied using as many x-ray intensities as possible.

Due to the fact that in most diffractive processes the phase is lost and crystal structure determination is, in principle, a trial-and-error procedure, whereby the observed intensities are to be matched to the intensities calculated from structural models. The procedures necessary for a detailed structure determination are beyond the scope of this article. A summary of the modern methods of structure refinements by x-ray methods may be found in the book of LUGER.



a. ZSM-5



b. ZSM-11

Figure 2.26 Schematic drawing of the channel system of ZSM-5 and ZSM-11

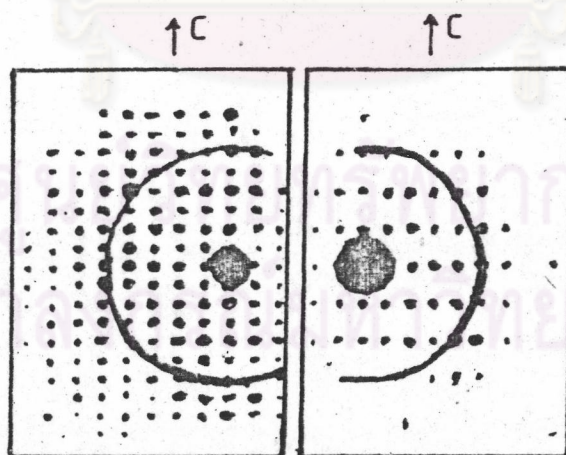


Figure 2.27 Schematic drawing of the electron diffraction pattern of the $h0l$ zones of erionite (left) and offretite (right)

The problems which occur especially in the case of zeolite have been summarized by Fischer [23].

One of these difficulties is given by the determination of the exact space group symmetry. This difficulty has its origin mainly in the scattering factors of the Si- and Al- atoms which are very similar due to the similar electron density surrounding these atoms. Therefore, the distribution of these atoms in the alumo-silicate framework seems to be random in most cases and the space group appears to have higher symmetry than is actually the case. If the refinement is done using a space group with an average Al-O- and Si-O-distance which is too symmetric, then ordering effects may be overlooked.

For difficulties of this kind the application of electron diffraction is advantageous.

A further problem is in the stacking faults possible in the various families of zeolites.

Figure 2.27 shows a schematic drawing of the $h01$ zones of erionite and offretite. It can be distinctly seen that every second row of the 1-reflexes is missing in the offretite system. In synthetic samples called zeolite T streaks parallel to c can be observed indicating disorder in the layers of sixmembered rings from which both structures can be constructed.

By the localization of cations inside the cavity systems of various zeolite structures further problems occur. The literature which has been published in this field up to now has been summarized with the most recent results in the atlas by Mortier [9]. Table 2.10 are shown x-ray powder data for some synthetic zeolites

2.6.2 The inspection of Crystal Size and Crystal Shape

[9]

A visual inspection of zeolite crystals and the inspection

Table 2.10a X-ray diffraction data for zeolite ZSM-2			Table 2.10b X-ray diffraction data for zeolite ZSM-3			
<i>hkl</i>	<i>d</i> (Å)	<i>I</i>	<i>d</i> (Å)	<i>I</i>	<i>d</i> (Å)	<i>I</i>
002	14.0	83	15.26	62	4.49	5
200	13.8	76	14.16	124	4.38	51
210	12.2	42	13.19	26	4.19	14
310	8.70	47	11.86	4	4.16	6
321	7.34	37	9.21	2	4.11	13
004	7.07	41	8.75	44	3.99	1
400	6.85	8	8.00	3	3.96	2
005	5.63	85	7.61	9	3.93	7
500	5.48	10	7.41	32	3.85	14
430			7.22	7	3.78	19
510	5.37	16	7.03	15	3.72	23
501			6.89	2	3.52	1
431			5.94	4	3.47	10
440	4.86	5	5.72	37	3.40	10
225			5.67	25	3.31	42
006	4.70	16	5.48	6	3.22	16
530			5.15	4	3.18	17
600	4.56	7	5.02	7	3.02	60
602	4.34	55	4.90	3	2.98	11
335	4.24	5	4.82	2	2.92	31
425	4.14	35	4.78	2	2.87	10
631	4.04	43	4.75	18	2.85	8
107	3.97	7	4.70	1	2.80	9
227	3.71	11	4.62	3	2.73	11
642	3.66	39	4.58	1	2.70	11
535	3.60	10				
650	3.51	4				
652	3.40	11				
218	3.38	16				
733	3.36	8				
653	3.28	27				
308						
715	3.19	8				
555						
527	3.15	41				
753	3.01	100				
920	2.97	16				
760						
726	2.94	18				
850	2.90	22				
930	2.88	3				
852	2.84	5				
904	2.79	9				
816	2.75	10				
746						
3,0,10	2.69	23				
952	2.61	6				

Table 2.10c X-ray diffraction data for zeolite ZSM-4		Table 2.10d X-ray diffraction data for zeolite ZSM-5				Table 2.10e zeolite ZSM-8		Table 2.10f zeolite ZSM-10	
$d(\text{Å})$	I	hkl	$d(\text{Å})$	I	hkl	$d(\text{Å})$	I	$d(\text{Å})$	I
16.07	w	200	11.36	s	610	3.84	vs	15.85	58
9.12	s	210	10.20	ms	611	3.74	vs	13.92	42
7.90	m	002	9.90	-	540	3.62	s	10.22	13
6.92	m	102	9.14	vw	315	3.50	w	7.87	22
5.99	ms	202	7.54	w	630	3.46	w	7.55	56
5.37	vs	212	7.17	w	603	3.33	w	7.04	13
5.28	w	311	6.79	vw	632	3.27	vw	6.29	35
4.70	ms	302	6.06	w	642	3.07	w	5.96	22
4.39	vw	203	5.77	w	513	3.00	w	5.46	31
3.93	w	410	5.63	w			m	5.25	15
3.79	s	411	5.42	vw				5.06	25
3.71	w	420	5.19	vw				4.50	76
3.62	w	303	5.05	vw				4.41	67
3.52	ms	500,	4.65	w				4.32	27
3.44	w	430	4.40	w				3.87	91
3.15	w	413	4.30	w				3.64	100
3.08	m	440,	4.12	vw				3.54	56
3.04	w	314						3.47	25
2.92	w	441	4.04	vw				3.42	27
2.65	w							3.32	13
2.62	w							3.22	16
2.52	w							3.16	31
2.37	w							3.10	67
2.28	w							3.04	73
2.14	vw							2.89	89
2.10	vw							2.73	48
2.08	vw							2.69	15
2.03	vw							2.57	15
1.98	w								

Tetragonal $a = 23.2\text{Å}$, $c = 19.9\text{Å}$

using a weakly enlarging instrument, such as a magnifying glass is important for geologists out in the field. In most cases, especially when inspecting synthetic zeolites, a microscope is needed. A microscope is usually used as a first means of identification by looking at the crystal shape of some specific zeolites. The shape of the crystals may sometimes be misleading because it depends on the conditions of growth. More detailed information on the crystal classification may be obtained using a polarization microscope. A very impressive example of the use of the optical microscope may be found in the kinetic studies of an x-type zeolite published in a paper by Zhdanov and Samulevich. These authors collected about 20 of the largest crystals, out of a batch of growing NaX-crystals, and observed their further growth under the microscope. From the increase of the crystal size they obtained the linear growth rate. At the end of the crystallization a representative sample of the product was taken and a histogram of the crystal size distribution was obtained from microscopic measurements. Extrapolating this distribution function with the growth rate which has previously been determined, the kinetics of the nucleation and the kinetics of the growth of the zeolite can be obtained.

In the field of electron optical instrumentation a wide range of techniques is available giving information concerning crystal habit and crystal size and other more specific characteristics. The recent literature in this field has been summarized by Baird. The main techniques used in zeolite research are connected to transmission electron microscopy (TEM), whereby the technique yielding most information is connected with the use of the scanning electron microscope (SEM) accompanied by a scanning micro-probe analysis.

With the transmission electron technique magnification up

to about 10^6 can be obtained corresponding to a point to point resolution of about 3 Å. Depending on the sample, this resolution can be improved by using special imaging techniques known as bright-field, dark field, or lattice imaging. In the scanning electron technique a fine beam of electrons is scanned over the surface of the sample using a system of deflection coils. The various signals produced by the interaction of the electron with the surface, such as secondary electrons, back scattered electrons, or x-rays can be used to form an image. Magnifications in the range of 20-50,000 are available with a resolution of about 100 Å. Non-metallic samples are usually covered with a thin film of carbon and gold to ensure a sufficient electric conductivity to prevent a surface charge which leads to distorted pictures. Another effect is the protection of heat sensitive material.

The output of the secondary electron varies according to the accelerating voltage of the beam (5-50 kv) and the structural characteristics of the sample as well as the particular angle of the incident beam with respect to the surface features. The changes in the secondary electron current induced by these features exhibit therefore a 3-dimensional character of the image.

The back-scattered electrons give a signal varying with the respective atomic number. Measuring the wave length of the induced characteristic x-ray radiation with special detectors an elementary analysis of the area hit by the beam can be carried out. This technique is known as electron micro-probe analysis.

In principle, this scanning technique and the analysis of the characteristic x-ray radiation can also be applied in transmissions. This method is usually called "Scanning Transmission Electron Microscopy" or STEM. This method has the advantage of better resolution as compared with the TEM, but has the disadvantage of difficult sample

preparation.

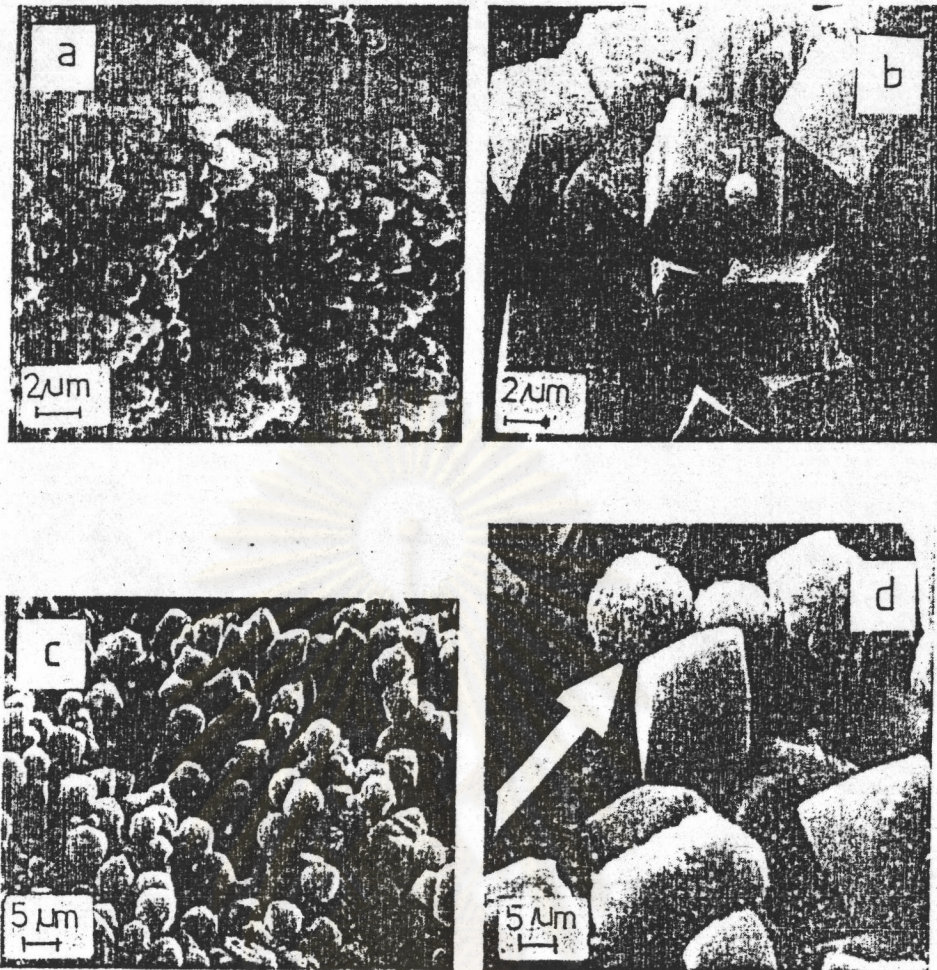
The most powerful method in the investigation of zeolite problems is the scanning electron microscopy (SEM). This method has above all the advantage of a simple preparation of the samples and gives quick information on the shape and the distribution of the size of the crystals and also of the presence of amorphous material.

In fig. 2.28 an example for the use of the SEM in zeolite synthesis is given. The picture shows two examples of A- and X-type zeolites which were grown from batches with very similar composition, varying only in the excess of alkali. A higher excess of alkali leads to a higher rate of nucleation and finally to smaller particles. The A-zeolite crystallizes in well-defined cubes which are sometimes truncated by octahedral planes, depending on the condition of growth. The X-zeolite crystallizes in octahedra. Figure 2.28d shows the X-crystal balls of agglomerated smaller crystals which are typical for the P-type zeolite which often occurs as an impurity during the crystallization of faujasite-type zeolites especially with higher Si/Al-ratios.

In summary it may be said that by inspecting a zeolite sample with the appropriate instrument, the shape of the crystal, the type of zeolite, and the impurities which are present in the sample may be identified. By observing the time dependency of the crystal size kinetic studies are also possible. Furthermore, special techniques such as electron-microscopy yield detailed information on the distribution of single components in the sample. By using high-resolution TEM-techniques structural details of the zeolite lattice may be resolved.

2.6.3 The Infrared Spectroscopy and The Framework Structure of Zeolites [9, 24]

Beside the diffraction methods the infrared spectroscopy has gained some importance for the structural characterization of



- | | | | | | | | | |
|----|------------------|-----|-----------------------|----------------|---------------------|----------------------|----------------------|-----------|
| a. | NaAlO_2 | 0.8 | Na_2O | SiO_2 | 40 | H_2O | A zeolite | |
| b. | NaAlO_2 | 0.8 | Na_2O | SiO_2 | 200 | H_2O | A zeolite | |
| c. | NaAlO_2 | 1.5 | SiO_2 | 1.37 | NaOH/SiO_2 | 100 | H_2O | X zeolite |
| d. | NaAlO_2 | 1.5 | SiO_2 | 1.37 | NaOH/SiO_2 | 150 | H_2O | X zeolite |

The P zeolite can be seen in the picture d, by the balls marked by the arrow.

Figure 2.28 Raster scan micrographs of A and X zeolites from batches with different alkalinity causing a different rate of nucleation and different particle size.

zeolites, especially in situations where no unambiguous x-ray patterns can be obtained.

The most important arguments for the application of this method are the straightforward sample preparation and an instrumentation which is readily available in many laboratories.

The object of this study was to apply mid-infrared spectroscopy to zeolite structural problems with the ultimate hope of using infrared, a relatively rapid and readily available analytical method, as a tool to characterize the framework structure and perhaps to detect the presence of the polyhedral building units present in zeolite frameworks. The mid-infrared region of the spectrum was used (1300 to 200 cm^{-1}) since that region contains the fundamental vibrations of the framework $(\text{Si,Al})\text{O}_4$ tetrahedra and should reflect the framework structure. Infrared data in similar spectral regions have been published for many mineral zeolites and a few synthetic zeolites [48]. There is an extensive literature on infrared spectra of silica, silicates, and aluminosilicates. However, no systematic study of the infrared characteristics of zeolite frameworks as related to their crystal structure has appeared.

The majority of the infrared transmission spectra were obtained using the KBr wafer technique. Spectra of at least 2 and often more preparations of each zeolite were obtained before the spectrum was accepted as being characteristic of the zeolite species. Spectra also were obtained using CsI wafers and in the case of several zeolites with mineral oil mulls and pure zeolite self-supported wafers, to establish any matrix effect. Only minor spectral variations were observed among the several techniques and matrices. Except where otherwise noted, the spectra reported here are for hydrated zeolites in KBr or CsI wafers. A typical wafer concentration was 0.5 mg of zeolite in 300 mg of KBr or -

CsI, however, zeolite concentration sometimes was varied to obtain the desired absorbance or to increase the sensitivity to weak bands. Spectra were determined with a Perkin Elmer Model 621 double beam grating spectrometer. Essentially identical spectra were obtained using a Perkin Elmer Model 225 double beam grating spectrometer and a Beckman Model IR-12 double beam grating spectrometer as were obtained with the P-E 621 for zeolites A, X, and Y. A few spectra were measured for dehydrated zeolites by activating the zeolite powders in air at 350°C, rapidly quenching into dry mineral oil, and running the spectrum as a mineral oil mull. Dehydration studies reported for Ca-exchanged Y zeolite using self-supported wafers were carried out with a cell and technique essentially the same as the described by Angell and Schaffer [49]. The spectral resolution is better than 5 cm^{-1} and the estimated accuracy $\pm 5\text{ cm}^{-1}$ using the same technique and instrument, but can be as high as $\pm 10\text{ cm}^{-1}$ with other measurement variations.

All of the synthetic zeolites investigated were prepared in this laboratory with the exception of the Zeolon product and ZK-5, and were fully characterized in terms of chemical composition, x-ray, and adsorption purity. All represent zeolite contents of greater than 90% and contained no crystalline impurities detectable by x-ray powder diffraction analysis. The Na "Zeolon" used was obtained from the Norton Co., and the experimental sample of ZK-5 was prepared by K.R. Muller at the Union Carbide European Research Associates Laboratory in Brussels, Belgium.

In the thermal decomposition studies of A, X, Y, and L, zeolites, powder samples of each zeolite were heated in ambient air for 16 hours at increasing temperatures to yield a series of thermal decomposition products with successively lower residual zeolite x-ray crystallinity. The heated powders were hydrated at room temperature and

run as KBr wafers to obtain their infrared patterns.

Infrared spectra were obtained on the synthetic zeolites A, N-A, X, Y, B(P1), KZ-5, omega (Ω), S,R,G,D,T,L,W, synthetic analogues of mordenite ("Zeolon"), and analcime (C), and for the related synthetic feldspathoid phases, hydroxy sodalite (HS) and hydroxy cancrinite (HC). The IR spectra are shown in figs. 2.29-2.34 and spectral frequencies listed in table 2.11. The definition of secondary building units (SBU) and building blocks used here is not as precise as that of Meier and there is some minor variation from Meier's structural classification. The zeolites were chosen to represent a spectrum of structural types and SBU and polyhedral building units in the frameworks as well as a range of Si, Al framework compositions.

Correlation of the infrared spectra with zeolite structure has led us to propose the following interpretations and hypotheses. Each zeolite species has a typical infrared pattern. In addition, there are often general similarities among the spectra of zeolites with the same structural type and in the same structural group. The infrared spectra of zeolites in the $1300-200\text{ cm}^{-1}$ region appear to consist of 2 classes of vibrations: those caused by internal vibrations of the framework TO_4 tetrahedron, the primary building unit in all zeolite frameworks, which tend to be insensitive to variations in framework structure, and vibrations related to external linkages between tetrahedra which are sensitive to the framework structure and to the presence of some SBU and building block polyhedra such as double rings and the large pore openings. No vibrations specific to AlO_4 tetrahedra or Al-O bonds are assigned but rather vibrations of TO_4 groups and T-O bonds where the vibrational frequencies represent the average Si, Al composition and bond characteristics of the central T cation. The proposed infrared assignments are presented in detail in table 2.12 and

Table 2.11 Infrared spectral data for synthetic zeolites

Zeolite	$\frac{\text{SiO}_2}{\text{Al}_2\text{O}_3}$	Asym. Stretch	Sym. Stretch	Dht. Rings	T-O Bend	Pore Opening?
A	1.88	1090vwsh	660vw	57ms	461m	378ms
Ca-A	1.9	1120vwsh	703vwsh	512ms	467m	370m
N-A	3.58	1131vwsh	675vw	572ms	474m	385m
N-A	6.01	1151vwsh	698vw	581ms	475m	393m
X	2.40	1060mb	690wsh	577m	458ms	365m
Y	3.42	1135msh	696m	561m	460ms	372m
Y	4.87	1130msh	714m	572m	453ms	380m
La-Y	5.0	1135msh	705m	569m	450ms	382m
Y	5.63	1130msh	789m	575m	456ms	383m
B(P)	2.8	1105msh	738mw	677m	435ms	380mwsh
Hydroxy sodalite (HS)	2.0	1096vwsh	723m	461ms	432ms	282vw?
Q	7.7	1130wsh	805mw	610mw	451ms	372m
ZK-5	6.0	1159wsh	730mw	572m	445m	408wsh
R	3.25	1136mwsh	738w	625m	452m	370vwsh
G	5.44	1138mwsh	720w	632m	460m	378vwsh
D	4.62	1184mwsh	755wsh	631m	430m	370vwsh
S	2.5	1110wsh	770vwsh	623 } mb 589sh } mb	448m	370vwsh
T	7.0	1156wsh	771w	631mw	467ms	366wsh
Hydroxy cancrinite (HC)	2.0	1085mw	755w	621m	458ms	353wb
I	6.0	1160wsh	721mw	580wsh	410vwsh	375vwsh
C	4.0	1162vwsh	740m	615vw	435wsh	375vwsh
Zecolon	9.95	1216w	795 } wb 772 } wb	621w	442ms	370vwsh
W	3.6	1129msh	786 } mw 756 } mw	571 } w 555 } w	448ms	370vwsh
			691mwsh	590wb	432ms	375vwsh
			691mwsh	512vwsh	432ms	375vwsh
			691mwsh	453vwsh	432ms	375vwsh

ms = strong; ms = medium strong; m = medium; mw = medium weak; w = weak; vw = very weak; sh = shoulder; b = broad.

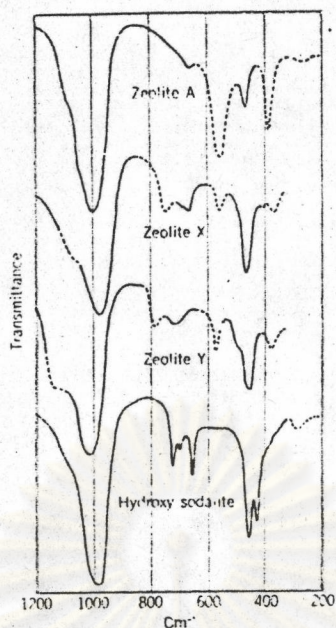


Figure 2.29 Infrared spectra of zeolites A, X, and Y and hydroxy sodalite(HS); Si/Al in X is 1.2 and in Y is 2.5

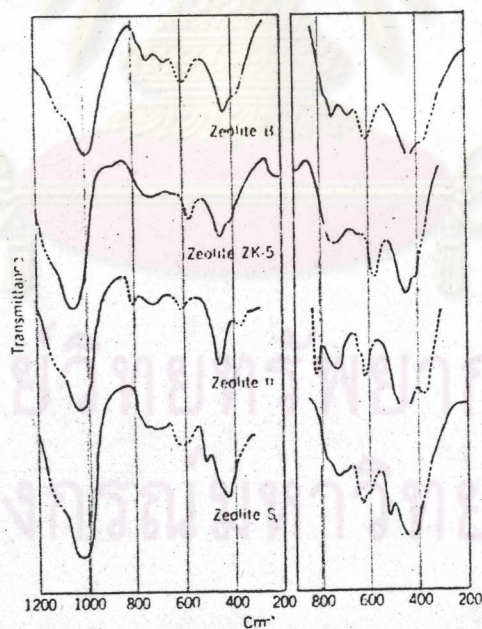


Figure 2.30 Infrared spectra of zeolites B(Pl), , and S ; right hand portion of figure represents a higher zeolite concentration in the wafer than in the left portion for figs. 2.30, 2.33, and 2.35

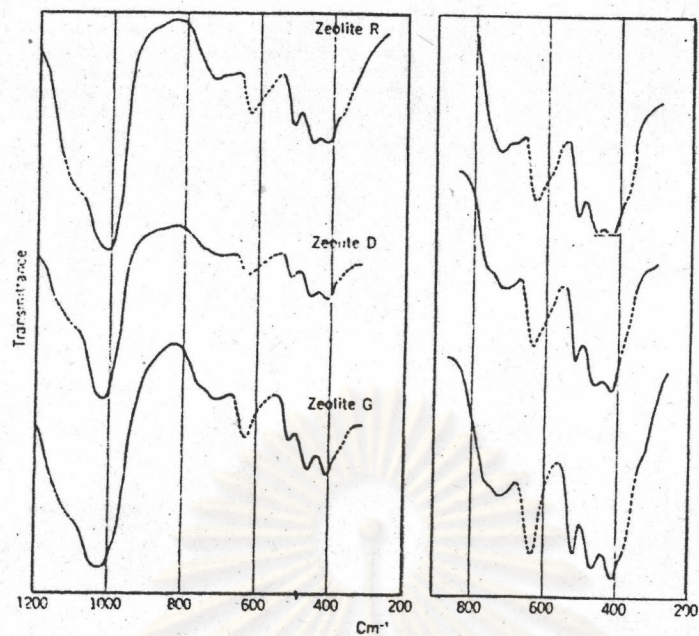


Figure 2.31 Infrared spectra of zeolites R, G, and D

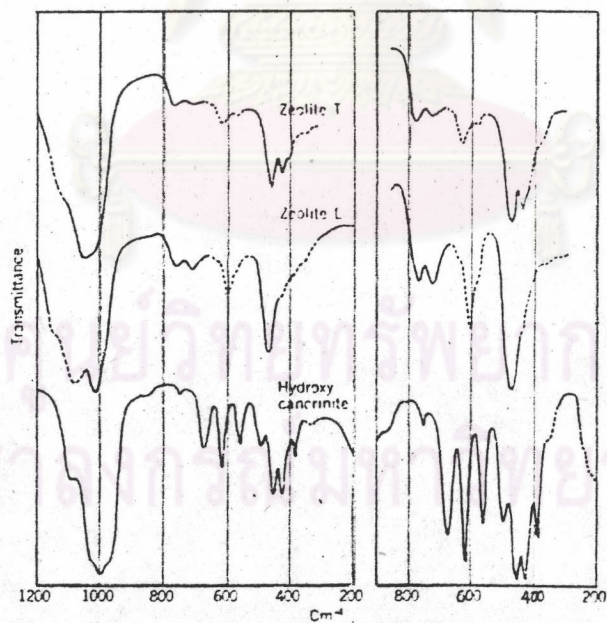


Figure 2.32 Infrared spectra of zeolites T, L, and hydroxy cancrinite(HC)

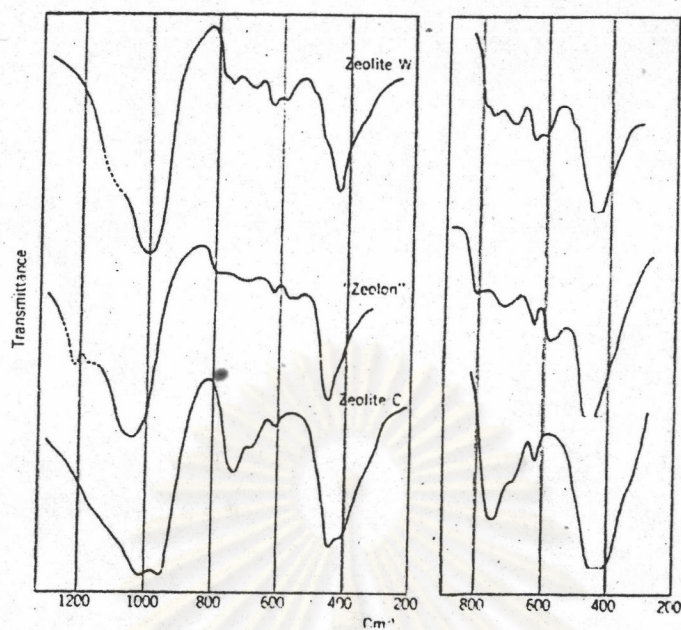


Figure 2.33 Infrared spectra of zeolites W, C, and Zeolon

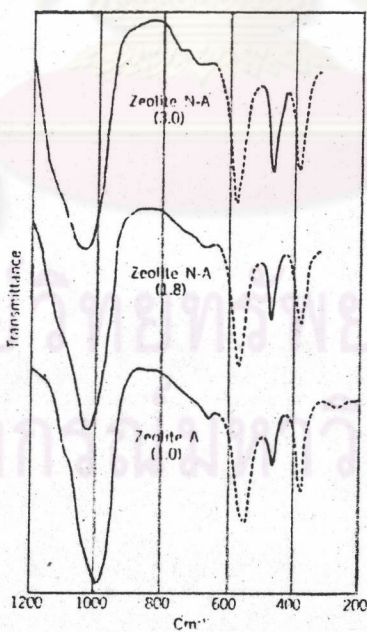


Figure 2.34 Infrared spectra of zeolites A and N-A ; numbers in parenthesis are Si/Al values

illustrated with the infrared spectrum of zeolite Y in fig. 2.35. The bands assigned to internal tetrahedral vibrations are shown in the figures with a full line drawing and those to external linkage modes with a broken line.

Table 2.12 Zeolite Infrared Assignments, cm^{-1}

Internal Tetrahedra		External Linkages	
Asym. stretch	1250-950	Double ring	650-500
Sym. stretch	720-650	Pore opening	300-420
T-O bend	420-500	Sym. stretch	750-820
		Asym. stretch	1050-1150 sh

From the bands summarized in table 2.12 the two most intense bands are at $950-1250 \text{ cm}^{-1}$ and at $420-500 \text{ cm}^{-1}$. These are common for all zeolites. The first is assigned to an asymmetric stretching mode and the second to a bending mode of the T-O bond. The bands in the region of $650-720 \text{ cm}^{-1}$ are assigned to a symmetric stretching within the TO_4 -tetrahedra. All other bands are more or less distinctly dependent on the crystal structure. This can be seen from the following fig. 2.34 where samples of the A structure with different Si/Al ratios are compared.

For all zeolites a nearly linear decrease has been observed for the asymmetric stretch band near 980 to 1100 cm^{-1} with increasing fraction of Al in the tetrahedral sites, as can be seen from fig. 2.34.

In the region of the external bands, a medium strong band near $500-650 \text{ cm}^{-1}$ is present in all structures with double rings as e.g. zeolite A, the faujasites, chabazite, gmelinite and the offretite-erionite system. Zeolites without double rings show only weak intensities in this region. Inconsistencies are observed with the

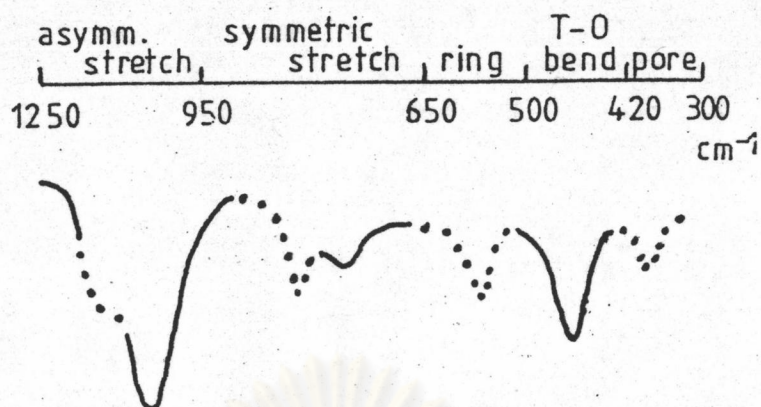


Figure 2.35 Assignments of the different infrared wave number regions with a spectrum of zeolite Y. Solid lines : internal tetrahedra, structure insensitive. Dotted lines : external linkages, structure sensitive

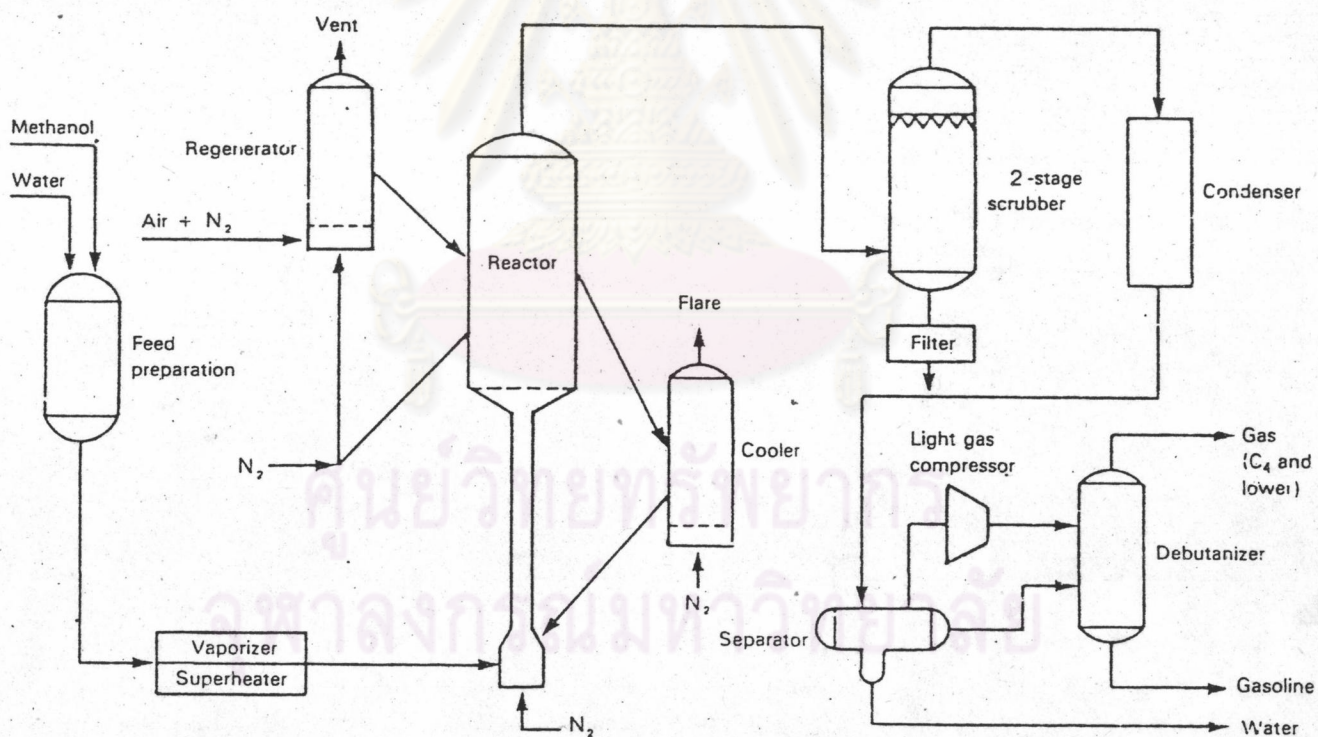


Figure 2.36 Fluidized-bed methanol to gasoline process

structures of P and Omega, which contain no double rings.

For the band of double sixmembered rings an influence of the Si/Al-ratio of the zeolite could be observed.

Further, distinct dependencies of the lattice vibrations on the cations in the zeolite could be established in the symmetric stretching region as well as in the bending vibrations of the TO_4 -tetrahedra.

Especially de Kanter et al. [9] were able to demonstrate linear relationships of several types of bands from the reciprocal sum of the radii of the O^{2-} -ion and the respective cation. From investigations of this kind informations on the cation distribution within the zeolite lattice can be obtained. An important application of the lattice vibrations in the midinfrared region is the investigation of nucleation mechanisms during the crystallization of zeolites. In the paper of Flanigen [9] a series of spectra of growing NaX is demonstrated, showing typical bands of the faujasite from the initial gel to the well crystallized sampled. Especially mentioned is a band near 575 cm^{-1} which may be assigned to double sixmembered rings.

Furthermore, two papers of Jacobs et al, [7] and Coudourier et al. shall be mentioned using IR-spectroscopy for the identification of small particles of ZSM-zeolites, showing no x-ray pattern but the typical effects of the catalytic activity of these substances. This activity could be closely related to the presence of a band near 550 cm^{-1} from which also an analysis of the quantity of the zeolite could be carried out.

2.7 Industrial Uses and Applications

According to Mumpton [3], zeolites were first used 2,000 years ago for building stones. The ion-exchange capability of zeolites was first investigated about 100 years ago; the molecular sieving capability

for separating gases, 40 years ago; and the first commercial uses of synthetic zeolites, 30 years ago. Breck [3] reported that, in 25 years, zeolites had achieved worldwide recognition as evidenced by the appearance of about 1,000 publications a year, and the recognition of 40 natural zeolite minerals and over 150 synthetic zeolites. Still, in 1977, only 10% of the known natural zeolites had commercial applications and fewer than 10% of the synthetic zeolites were successfully marketed. Flanigen reported that the major use of natural zeolites is in bulk mineral applications: in Europe in the building and construction industry, where proximity to building location makes them cost effective, and in the Far East as filler in the paper industry, largely because of the unavailability of alternate mineral resources. A modest market for zeolite minerals has developed as a molecular sieve adsorbent in acid gas drying in the natural gas industry, in NH_4 removal in water treatment systems by ion exchange, and in the production of oxygen and nitrogen via adsorptive air separation, especially in Japan. In general, however, their penetration into molecular sieve applications has been quite limited. Zeolite applications are summarized as follows [8]:

Adsorption:

Regenerative processes: Separations based on sieving
 Separations based on selectivity.

Purification

Bulk separations

Nonregenerative process: Drying

Windows

Refrigerants

Cryosorption

Ion exchange:

Regenerative process: NH_4^+ removal
 Metal separations, removal from waste water

Nonregenerative processes: Radioisotope removal and storage
 Detergent builder
 Artificial kidney dialysate regeneration
 Aquaculture- NH_4^+ removal
 Ruminant feeding of nonprotein-nitrogen (NPN)
 Ion-exchange fertilizers

Catalysis:

Hydrocarbon conversion: Alkylation
 Cracking
 Hydrocracking
 Isomerization

Hydrogenation and dehydrogenation

Hydrodealkylation

Methanation

Shape-selective reforming

Dehydration

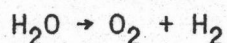
Methanol to gasoline

Organic catalysis

Inorganic: Hydrogen sulfide oxidation

Ammonia reduction of nitric oxide

Carbon monoxide oxidation



Ammonium removal from municipal wastewater

In early studies of the use of ion exchange for wastewater

ammonia removal, a permutite type exchanger and various organic resin ion exchangers were found to have poor selectivity for ammonium ions resulting in unacceptably low ammonium loadings and low regeneration efficiency, corresponding high costs, and problems of brine disposal.

This situation was altered dramatically by a report by Ames [9] which presented data showing the superior ammonium ion selectivity of several zeolite ion exchangers tested. Clinoptilolite and Union Carbide's AW 400 were most promising. Subsequent pilot plant tests using clinoptilolite demonstrated ammonium removal greater than 95%. Regeneration was accomplished using a lime salt solution which was effectively reused after ammonia was removed from the regenerant solution by air stripping and exhausted to the atmosphere. An improved process (the ARRP Process) for the rejuvenation of the regenerant solution at elevated pH levels, followed by the removal of the NH_3 from the air by acid scrubbing, and recycling the air to the stripper was developed later. All of these developments were reviewed in detail elsewhere.

Molecular Sieve Zeolite builders in Detergents

The prime function of phosphates in detergents is to reduce the activity of the "hardness" ions, Ca^{++} and Mg^{++} , in the wash water by complexing. Zeolite ion exchangers in powder form can also provide this service by removing Ca^{++} and Mg^{++} from the solution and replacing them with "soft" ions such as Na^+ [9]. Heavy duty powder detergents employing the Na form of the LINDE. A zeolite in low or zero phosphate formulations are already being sold in several areas of the United States, Europe, and elsewhere. This use has grown rapidly and now consumes hundreds of millions of pounds of zeolites annually worldwide.

This application has been developed primarily by scientists at Henkel in Germany and Procter and Gamble in the United States. The

literature on this application, especially the patent literature, is voluminous and specialized. It will not be reviewed in detail here. Instead the discussion will be limited to the related ion exchange behavior of zeolites.

Conversion of Methanol over Zeolite Catalysts

In view of the latest critical energy situation in the Western world, extensive research is being conducted to reconsider the potentialities of other non-petroleum materials to become important sources of fuels.

Methanol, a potential motor fuel, is one among the products readily formed in large amounts, from coal or synthesis gas, by existing technologies. It can be either used directly as a fuel in automotive engines, or be blended with gasoline.

The formation of hydrocarbons from methanol was first reported over classical NaX zeolites [9] and, since then, over a large variety of acidic zeolitic or non-zeolitic catalysts [9].

A novel process for the straightforward conversion of methanol to gasoline over ZSM-5 zeolite catalyst has been recently developed by Mobil Oil Co. [3, 9]. It is commonly referred to as "Methanol-to-Gasoline" (MTG) process.

The Mobil Corp.'s methanol-to-gasoline (MTG) process using its ZSM-5 zeolite now has an operating plant in New Zealand. This plant has a fixed-bed reactor. The fluidized-bed process for MTG conversion has been declared successful after the completion of the final phase of operation at a pilot plant at Wesseling, Federal Republic of Germany. The raw gasoline yield is 90% with an octane rating of 90.25. The fluidized-bed process, shown in fig. 2.36 is reported to significantly improve the MTG process and possibly permit feedstocks other than methanol to be used.

Radioactive Waste Storage

As discussed earlier, zeolites are employed in separations of long-lived Cs and Sr radioisotopes. These radioisotopes can also be retained on zeolites for long-term storage by ion exchange onto the zeolite, drying the zeolite to prevent excessive pressure after the container is sealed, and sealing the containers by welding [9].

Since zeolites contain alkali metal or alkaline earth oxides, alumina and silica (major constituents of many common glasses), heating to temperatures sufficient to cause destruction of the zeolite crystal structure can convert the zeolite to a glass. Addition of suitable flux calcining agents can allow this to be accomplished at lower temperatures. Leach rates for alkali and alkaline-earth elements from aluminosilicate glasses are extremely low (e.g., 10^{-7} g/cm²-day). The chemical durability, low leach rates, and high thermal conductivity of glass combine to make this an ideal form for immobilizing radioactive wastes.

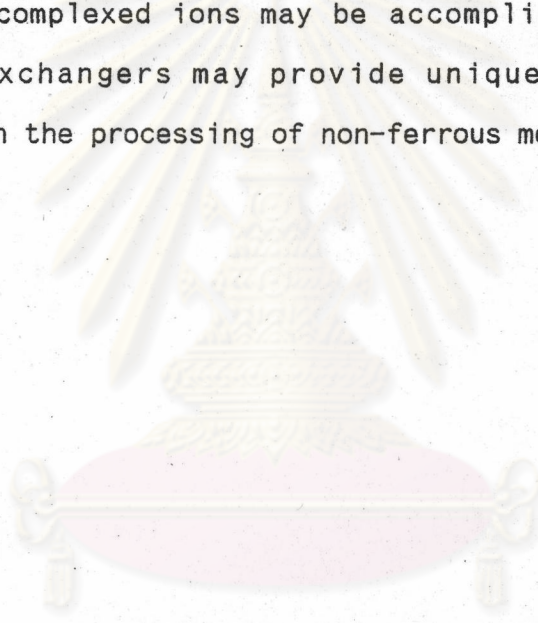
One process employs a hydrous metal oxide type cation exchanger (Na Ti₂O₅H) to trap ⁹⁰Sr and other radioisotopes from liquid wastes from fuel reprocessing, followed by a zeolite bed to trap the ¹³⁴Cs and ¹³⁷Cs. The ion exchangers are removed, blended, dried and hot-press-sintered to yield stable ceramic discs with low leach rates. The process has been tested at Hanford [9]. Similarly, radioactive Cs, Sr and Pu were sorbed on LINDE AW-500 zeolite for final solidification in concrete or glass.

Metal Removal, Recovery, and Separations[9]

Many zeolites exhibit high selectivities for various heavy metals and are under consideration for use in recovery of precious and semi-precious metals and for removal of heavy metals from industrial and metals processing waste waters.

Because of their availability (especially in Japan), the zeolites clinoptilolite and mordenite have been studied for heavy metals (especially Cd, Cu, Pb, and Zn) removal from waste waters. The high selectivities of several zeolite ion exchangers for Ag^+ also suggests their use for the recovery of silver from waste waters.

Separations and purifications of non-ferrous metals may also be accomplished by zeolite ion exchange. For example, Breck reported the unique separation of Co^{++} and Ni^{++} and LINDE Type A zeolite. Many other separations of non-ferrous metals are also possible. Separations of both free and complexed ions may be accomplished, suggesting that zeolite ion exchangers may provide unique new separations and purifications in the processing of non-ferrous metals.



ศูนย์วิทยทรัพยากร
จุฬาลงกรณ์มหาวิทยาลัย